

THE SEEDS HIGH CONTRAST IMAGING SURVEY OF EXOPLANETS AROUND YOUNG STELLAR OBJECTS

TAICHI UYAMA¹, JUN HASHIMOTO², MASAYUKI KUZUHARA³, SATOSHI MAYAMA⁴, EIJI AKIYAMA⁵, THAYNE CURRIE⁶, JOHN LIVINGSTON¹, TOMOYUKI KUDO⁶, NOBUHIKO KUSAKABE², LYU ABE⁷, WOLFGANG BRANDNER⁸, TIMOTHY D. BRANDT⁹, JOSEPH C. CARSON^{10,8}, SEBASTIAN EGNER⁶, MARKUS FELDT⁸, MIWA GOTO¹¹, CAROL A. GRADY^{12,13,14}, OLIVIER GUYON⁶, YUTAKA HAYANO⁶, MASAHIKO HAYASHI¹⁵, SAEKO S. HAYASHI⁶, THOMAS HENNING⁸, KLAUS W. HODAPP¹⁶, MIKI ISHII¹⁵, MASANORI IYE¹⁵, MARKUS JANSON¹⁷, RYO KANDORI¹⁵, GILLIAN R. KNAPP¹⁷, JUNGMI KWON¹, TARO MATSUO¹⁸, MICHAEL W. MCELWAIN¹², SHOKEN MIYAMA¹⁹, JUN-ICHI MORINO¹⁵, AMAYA MORO-MARTIN^{17,20}, TETSUO NISHIMURA⁶, TAE-SOO PYO⁶, EUGENE SERABYN²¹, TAKUYA SUENAGA^{15,22}, HIROSHI SUTO^{2,15}, RYUJI SUZUKI¹⁵, YASUHIRO H. TAKAHASHI^{1,15}, MICHIIHIRO TAKAMI²³, NARUHISA TAKATO⁶, HIROSHI TERADA¹⁵, CHRISTIAN THALMANN²⁴, EDWIN L. TURNER^{17,25}, MAKOTO WATANABE²⁶, JOHN WISNIEWSKI²⁷, TORU YAMADA²⁸, HIDEKI TAKAMI¹⁵, TOMONORI USUDA¹⁵, AND MOTOHIDE TAMURA^{1,2,15}

Draft version January 2, 2017

ABSTRACT

We present high-contrast observations of 68 young stellar objects (YSOs) explored as part of the SEEDS survey on the Subaru telescope. Our targets are very young (<10 Myr) stars, which often harbor protoplanetary disks where planets may be forming. We achieve a typical contrast of $\sim 10^{-4}$ – $10^{-5.5}$ at an angular distance of $1''$ from the central star, corresponding to typical mass sensitivities (assuming hot-start evolutionary models) of $\sim 10 M_J$ at 70 AU and $\sim 6 M_J$ at 140 AU. We detected a new stellar companion to HIP 79462 and confirmed the substellar objects GQ Lup b and ROXs 42B b. An additional six companion candidates await follow-up observations to check for common proper motion. Our SEEDS YSO observations probe the population of planets and brown dwarfs at the very youngest ages; these may be compared to the results of surveys targeting somewhat older stars. Our sample and the associated observational results will help enable detailed statistical analyses of giant planet formation.

¹ Department of Astronomy, The University of Tokyo, 7-3-1, Hongo, Bunkyo-ku, Tokyo, 113-0033, Japan

² Astrobiology Center of NINS, 2-21-1, Osawa, Mitaka, Tokyo, 181-8588, Japan

³ Department of Earth and Planetary Sciences, Tokyo Institute of Technology, Ookayama, Meguro-ku, Tokyo 152-8551, Japan

⁴ The Center for the Promotion of Integrated Sciences, The Graduate University for Advanced Studies (SOKENDAI), Shonan International Village, Hayama-cho, Miura-gun, Kanagawa 240-0193, Japan

⁵ Chile Observatory, National Astronomical Observatory of Japan, 2-21-2, Osawa, Mitaka, Tokyo, 181-8588, Japan

⁶ Subaru Telescope, National Astronomical Observatory of Japan, 650 North Aohoku Place, Hilo, HI96720, USA

⁷ Laboratoire Lagrange (UMR 7293), Université de Nice-Sophia Antipolis, CNRS, Observatoire de la Coted'azur, 28 avenue Valrose, 06108 Nice Cedex 2, France

⁸ Max Planck Institute for Astronomy, Königstuhl 17, 69117 Heidelberg, Germany

⁹ Astrophysics Department, Institute for Advanced Study, Princeton, NJ, USA

¹⁰ Department of Physics and Astronomy, College of Charleston, 66 George St., Charleston, SC 29424, USA

¹¹ Universitäts-Sternwarte München, Ludwig-Maximilians-Universität, Scheinerstr. 1, 81679 München, Germany

¹² Exoplanets and Stellar Astrophysics Laboratory, Code 667, Goddard Space Flight Center, Greenbelt, MD 20771, USA

¹³ Eureka Scientific, 2452 Delmer, Suite 100, Oakland CA96002, USA

¹⁴ Goddard Center for Astrobiology

¹⁵ National Astronomical Observatory of Japan, 2-21-1, Osawa, Mitaka, Tokyo, 181-8588, Japan

¹⁶ Institute for Astronomy, University of Hawaii, 640 N. Aohoku Place, Hilo, HI 96720, USA

¹⁷ Department of Astrophysical Science, Princeton University, Peyton Hall, Ivy Lane, Princeton, NJ08544, USA

¹⁸ Department of Earth and Space Science, Graduate School of Science, Osaka University, 1-1 Machikaneyamacho, Toyonaka,

Osaka 560-0043, Japan

¹⁹ Hiroshima University, 1-3-2, Kagamiyama, Higashihiroshima, Hiroshima 739-8511, Japan

²⁰ Department of Astrophysics, CAB-CSIC/INTA, 28850 Torrejón de Ardoz, Madrid, Spain

²¹ Jet Propulsion Laboratory, California Institute of Technology, Pasadena, CA, 171-113, USA

²² Department of Astronomical Science, The Graduate University for Advanced Studies, 2-21-1, Osawa, Mitaka, Tokyo, 181-8588, Japan

²³ Institute of Astronomy and Astrophysics, Academia Sinica, P.O. Box 23-141, Taipei 10617, Taiwan

²⁴ Swiss Federal Institute of Technology (ETH Zurich), Institute for Astronomy, Wolfgang-Pauli-Strasse 27, CH-8093 Zurich, Switzerland

²⁵ Kavli Institute for Physics and Mathematics of the Universe, The University of Tokyo, 5-1-5, Kashiwanoha, Kashiwa, Chiba 277-8568, Japan

²⁶ Department of Cosmosciences, Hokkaido University, Kita-ku, Sapporo, Hokkaido 060-0810, Japan

²⁷ H. L. Dodge Department of Physics & Astronomy, University of Oklahoma, 440 W Brooks St Norman, OK 73019, USA

²⁸ Astronomical Institute, Tohoku University, Aoba-ku, Sendai, Miyagi 980-8578, Japan

1. INTRODUCTION

Since the first convincing detection of an exoplanet around a main sequence star (Mayor & Queloz 1995), in 1995, about 3500 exoplanets have been confirmed. Surprisingly, many exoplanets, such as hot Jupiters and high-eccentricity planets, are quite different from those in the solar system (e.g. Mayor & Queloz 1995; Holman et al. 1997). Those unexpected exoplanets cannot necessarily be reproduced by conventional theories of planet formation, which were originally developed to explain the properties of the solar system (core accretion model; e.g. Hayashi et al. 1985). Such planet formation models (e.g. Ida et al. 2013) have been updated to help explain the myriad exoplanets discovered to date. Ongoing observations and characterizations of various exoplanets help test the updated models. Most of the planet detections to date have resulted from radial velocity (e.g. Mayor & Queloz 1995) and transit surveys (e.g. Auvergne et al. 2009; Batalha et al. 2011). These indirect methods observe stars and measure periodic fluctuations caused by the existence of orbiting planets. They are particularly effective for detecting exoplanets with shorter orbital periods, like less than 5 years.

Direct imaging is technically difficult due to the large dynamic range required to detect a planet that is $\sim 10^{-6}$ times fainter than the central star. However, with the development of adaptive optics (AO) on large, ground-based telescopes, the method has begun to successfully open up the previously unexplored parameter-space occupied by wide-separation, gas giants ($\sim 5\text{--}75 M_J$ and $\sim 10\text{--}1000$ AU). The number of exoplanets confirmed through direct imaging is still far fewer than those found through indirect methods, such as radial velocity or transit. However, direct imaging can reveal physical parameters (e.g. mass, temperature and atmosphere information; Currie et al. 2011) and orbital parameters (e.g. semimajor axis, inclination and eccentricity; Chauvin et al. 2012) of wide-orbit exoplanets that are poorly explored by indirect methods. As a result, direct imaging uniquely probes exoplanet populations that are effectively inaccessible by radial velocity and transit methods. The first directly-imaged planets—e.g. HR 8799 bcde; κ And b; β Pic b; GJ 504 b (Marois et al. 2008; Lagrange et al. 2010; Carson et al. 2013; Kuzuhara et al. 2013)—prove the extremes of planet formation. These planets, orbiting at $\sim 10\text{--}150$ AU and with masses of $M \sim 3\text{--}15 M_J$, are difficult to form by either core accretion or disk instability (Dodson-Robinson et al. 2009; Kratter et al. 2010; Currie et al. 2011). However, constraining the frequency and semimajor axis distribution of these planets may clarify which planet formation mechanism is responsible for their existence (Brandt et al. 2014a). Estimating physical parameters of detected exoplanets requires accurate age estimations of the host stars. Young stellar objects (YSOs) make appealing target populations in part because most of them are associated with star-forming regions whose ages are relatively well established ($\sim 1\text{--}10$ Myr).

Here we observe YSOs with direct imaging in an effort to detect young exoplanets with ongoing formation and to improve our understanding of how planets form in protoplanetary disks. Previous direct imagin re-

ported a few low-mass companions around YSOs such as GQ Lup b, ROXs 42Bb, and possibly LkCa 15 bc (Neuhäuser et al. 2005; Currie et al. 2014b; Sallum et al. 2015). Strategic Exploration of Exoplanets and Disks with Subaru (SEEDS; Tamura 2009), a project exploring exoplanets and circumstellar disks with Subaru/HiCIAO (Suzuki et al. 2010) and AO188 (Hayano et al. 2008), has conducted, from 2009 to 2015, a direct imaging survey of more than 400 targets. A main goal of SEEDS is to constrain formation and evolution scenarios of planetary systems, including not only exoplanets but also protoplanetary disks, from the point of view of direct imaging. To achieve this, SEEDS selected targets whose ages range from 1 Myr to a few Gyr, for systematic analyses of systems at different stages. Comparing information on exoplanets with various ages can be useful for placing constraints on their formation and evolution mechanisms.

SEEDS has several target categories: Young Stellar Objects, Moving Groups (Brandt et al. 2014b), Open Clusters (Yamamoto et al. 2013), Debris Disks (Janson et al. 2013), and Nearby Stars (Kuzuhara 2016, in prep.). We report here the observations and results from systematic explorations carried out in the YSO category. The sample selection of YSOs is described in Section 2. In Section 3, the observations and data reduction are presented for each target. Section 4 provides detection limit results and expanded information on individual targets. Preliminary statistical discussions are described in Section 5. Finally, we summarize our results in Section 6.

2. SAMPLE SELECTION

2.1. *Young Stellar Objects*

We define YSOs to be young stars with average ages less than ~ 10 Myr. Most of our targets show evidence for dusty circumstellar disks, ranging presumably from pre-planet building phases (optically thick, gas rich protoplanetary disks) to post-jovian planet building phases (optically thin, gas poor debris disks). Some spectral energy distribution (SED) data of YSOs show far-infrared (FIR) excess but little mid-infrared (MIR) excess (Strom et al. 1989). Disks showing such SED features are called “transitional disks” and have been predicted to have gaps, which may be a result of planet formation (Marsh & Mahoney 1992, 1993; Quanz et al. 2013a). Some such YSOs with transitional disks exhibit resolved gaps and accompanying structures (e.g. spiral arms) that may indicate hidden planets (Hashimoto et al. 2012; Muto et al. 2012; Grady et al. 2013; Thalmann et al. 2014; Currie et al. 2014c). In addition, a few young protoplanets have been imaged inside the gaps of transitional disks (Kraus & Ireland 2012; Currie et al. 2015). At near infrared (NIR) wavelengths, young planets are brighter than their older counterparts, so YSOs may be particularly well suited for simultaneously probing lower mass planets and protoplanetary disks (see Section 3 for details).

SEEDS adopts two imaging modes. One is most effective for disk searches while the other is more optimized for planet searches (see Section 3.1). The two methods can be combined to simultaneously study both planets and disks. The simultaneous study of disk and exoplan-

ets is helpful for analyzing the relationship between disk structures and planet formation. However, note that our SEEDS explorations are limited to exoplanets outside the gap region, due to self-subtraction effects (details are described in Section 3.2). Also, we are so far unable to conclude systematic relations between disk geometry and exoplanet frequency.

Section 4.3 provides the available individual SED and disk information for each YSO. Most of our YSO targets are located at distances larger than 100 pc. This is because almost all SEEDS/YSO targets belong to star-forming regions (SFRs) and active SFRs in the Milky Way are mainly located in Gould Belt (Dunham et al. 2015), which is farther than 140 pc. The targets of the YSO category are therefore fainter than those of other SEEDS categories, making the AO performance less effective. Also, the large distances make it more difficult to distinguish orbiting companions at a solar-system scale from the central star. However, as previously mentioned, our SEEDS data were optimized for studying disks, but can still place important constraints on giant planets.

2.2. SEEDS Target Selections

Table 2 lists all SEEDS/YSO data analyzed in this work and Figure 8 summarizes spectral types of the YSO targets. Hereafter the targets are sorted by their RAs.

We explain here the procedures to select our YSO targets. The guidelines and criteria are somewhat different for each SFR (see below for the details). However, we first describe the common target-selection procedures used for all the SFRs.

First, we searched the literature nearby SFRs observable from the summit of Mauna Kea. We aimed to select YSOs brighter than $R = 15$ to ensure high quality adaptive optics performance and therefore a sufficient angular resolution. We de-prioritized M-type YSOs due to a small frequency of gas giants expected around M dwarfs (Kokubo & Ida 2002). Famous and relatively bright sources that have been observed in various methods such as AB Aur are prioritized. The YSOs whose disks had been resolved before SEEDS observations are also prioritized. Our used catalogues are described in the sections for each SFR. Our SEEDS/YSO observations were largely divided into two effective surveys: disk survey and planet survey. The YSOs whose SEDs suggested a large, full disk were prioritized for disk study. Objects with transitional or debris disks were selected for both planet and disk explorations. Sources exhibiting little or weak IR excesses were slated for planet searches if they showed any youth indicators such as $H\alpha$ emissions, X-ray emissions, or Lithium absorptions. For each SFR, we adopted typical estimates for age and distance (see Table 1), which we later used to constrain potential exoplanet masses around the YSO. Most of our employed age estimations derived from isochrones of pre-main sequence evolutionary tracks (e.g. D’Antona & Mazzitelli 1994; Baraffe et al. 1998).

We below describe the basic procedures of target selection for individual SFRs. The majority of targets were selected before the SEEDS survey started, but we include in the subsequent summaries information published since then.

Taurus-Auriga — At the first step, we selected

YSOs with spectral types of B0–M1 (Strom et al. 1989; Beckwith et al. 1990; Kenyon & Hartmann 1995a; Andrews & Williams 2005; Furlan et al. 2006; McCabe et al. 2006; Najita et al. 2007). Subsequently, we removed close binaries that have separations between components are less than $3''$ (Beckwith et al. 1990; White & Ghez 2001a; White & Hillenbrand 2004; Furlan et al. 2006; McCabe et al. 2006; Najita et al. 2007). The YSOs fainter than $R = 15$ were also removed by checking the USNO-B1.0 catalog (Monet et al. 2003). The R -band magnitudes of Taurus-Auriga (hereafter Taurus) YSOs measured by our previous Subaru-AO observations (e.g., Fukagawa et al. 2004; Itoh et al. 2005) were additionally used to support the USNO-B1.0 photometry. Next, we investigated SEDs of all selected YSOs using *Spitzer* data (Hartmann et al. 2005; Calvet et al. 2005; Furlan et al. 2006; Padgett et al. 2006; Najita et al. 2007; Luhman et al. 2010; Espaillat et al. 2011) and radio observations (Kitamura et al. 2002; Andrews & Williams 2005) in order to find circumstellar disks. We also assign the higher priorities to the YSOs with the observations of resolved disks (Kitamura et al. 2002; Andrews & Williams 2007; Isella et al. 2010a; Karr et al. 2010, and references in Section 4.3). In particular, the transitional disks are the highest-priority targets. A transitinaol disk’s inner hole can be caused by grain growth and/or photoevaporation, as well as the influence of planet formation (Williams & Cieza 2011). The large inner hole ($> \sim 100$ AU) serves to significantly decrease the infrared continuum (Williams & Cieza 2011). Hence, objects detected at only longer wavelength (e.g. $> 850 \mu\text{m}$) have high priorities.

We examined CIAO (Subaru) and HST archival data to verify whether or not there are circumstellar structures such as nebular and companions around the targets. The stellar jets are closely related with the accretion disks (Blandford & Payne 1982) and thus we include YSOs which have the jet among disk survey targets.

Kenyon et al. (2008) summarized distance investigations of YSOs in Taurus-Auriga (hereafter Taurus), with the optimum estimate of 140–145 pc as this SFR’s distance. On the other hand, distances of Taurus members estimated from their parallaxes are distributed within ~ 130 –160 pc (Torres et al. 2007, 2009, 2012). We accordingly assume the Taurus-Auriga SFR’s distance to be 140 pc. We calculated the median and the standard deviation of Taurus-Auriga’s age using the results of Bertout et al. (2007) in which member’s ages are estimated with evolutionary tracks of Siess et al. (2000), resulting in 1.3–13 Myr. Küçük & Akkaya (2010) that carried out isochrone analyses with a large sample of YSOs in Taurus and found that the ages of those YSOs are best consistent to 1–3 Myr. Considering these studies, we adopt 1–13 Myr as the typical age of Taurus.

Upper Scorpius (Upper Sco) — R -band magnitudes for the Upper Sco region were compiled from the USNO-B1.0 catalog (Monet et al. 2003). To identify YSOs, we first investigated targets’ $H\alpha$ emission, Lithium absorption, and X-ray emission from Walter et al. (1994), Preibisch et al. (1998), and Köhler et al. (2000a), which

were also used to obtain their spectral types and R magnitudes. To compile the subset suitable for disk and planet explorations, we selected the young targets whose SEDs showed infrared excesses and/or a gap around 24 μm , as identified via *Spitzer* infrared data (Chen et al. 2005; Carpenter et al. 2006, 2009; Dahm & Carpenter 2009; Dahm 2010). A gap around 24 μm indicates that the inner part of the disk is cleared (Strom et al. 1989; Espaillat et al. 2014).

We assume an age of the Upper Sco SFR to be 9–13 Myr, based on Pecaute et al. (2012) who derived an age using a large sample of YSOs via not only isochrone but also other indicators such as lithium absorptions or $H\alpha$ emissions (Balachandran 1990; White & Basri 2003). de Zeeuw et al. (1999) and Bertout et al. (1999) measured individual distances of YSOs in Upper Sco with Hipparcos data and derived the typical value of 145 pc, which is used in this work.

ρ Ophiuchus — We first took stars of $R < 15$ in the ρ Ophiuchus area by investigating the literature (Wilking et al. 2005; Bouvier & Appenzeller 1992; Cieza et al. 2007; Zacharias et al. 2005). Next, in order to verify the youth of those stars, we attempted to collect the measurements of their $H\alpha$ emissions summarized in Wilking et al. (2005), Bouvier & Appenzeller (1992), and Martin et al. (1998). The previous observations of speckle interferometry (Barsony et al. 2003; Ratzka et al. 2005), adaptive optics (Cieza et al. 2010), and HST/NICMOS (Allen et al. 2002) helped us rule out close binary systems.

We also checked whether the target candidates have the circumstellar disks, because they may have such disks if they are young. The presences of the infrared excesses in the SEDs and the submillimeter emissions are indicators of circumstellar disk, so we examined if those indicators have been observed for our target candidates, using the *Spitzer* data (Cieza et al. 2007; Furlan et al. 2009; McClure et al. 2010; Cieza et al. 2010) and submillimeter observations (Andre & Montmerle 1994; Andrews et al. 2009). In selecting disk-bearing YSOs, we prioritized transitional disks, which are useful for both planet searches and disk studies. We used optical spectroscopy (Bouvier & Appenzeller 1992; Martin et al. 1998; Wilking et al. 2005) and IR spectroscopy (Luhman & Rieke 1999) to check the strengths of lithium absorption, which is also a youth indicator, and the spectral types of our target candidates.

We cite the distance and the age of Ophiuchus from Lombardi et al. (2008) and Greene & Meyer (1995). Lombardi et al. (2008) obtained precise distance of Ophiuchus and Lupus by combining Hipparcos data with extinction maps from Two Micron All Sky Survey (2MASS) data. Greene & Meyer (1995) estimated ages of members in Ophiuchus with several evolutionary

models. Greene & Meyer (1995) concluded that the age difference is comparable with observational uncertainties in determining stellar luminosities.

Lupus — Systematic sample selection in Lupus for SEEDS is not practical because of its low declination. We then include several intriguing objects based on millimeter / submillimeter observations (Hughes et al. 1994; Nuernberger et al. 1997; Wichmann et al. 1999; Joergens et al. 2001; Melo 2003; Merín et al. 2008; Comerón et al. 2009). They have strong emission at 1.3 mm that indicates the presence of a massive disk (e.g. Tsukagoshi et al. 2011).

As mentioned above, Lombardi et al. (2008) estimated distances for Lupus. The estimated typical value of 155 pc is consistent with Hughes et al. (1993). Hughes et al. (1994) used a large number of stars in Lupus to estimate ages using isochrone. The mode value is 3.2 Myr but the ages range from 0.1 Myr to 10 Myr (Hughes et al. 1994). We adopt 0.1–10 Myr in order to cover this range.

Corona Australis — We selected bright stars ($R < 15$ mag) that show the youth indicators (Wilking et al. 1997; Chini et al. 2003; Forbrich & Preibisch 2007), except close binaries (Köhler et al. 2008). We then evaluate priorities of each YSO and selected transitional disk targets (Hughes et al. 2010).

We adopt the age of Corona Australis (CrA) as 0.1–10 Myr from Neuhäuser et al. (2000). Previous studies showed CrA’s age is between ~ 1 Myr (Knacke et al. 1973) and 6 Myr (Wilking et al. 1992). Neuhäuser et al. (2000) estimated the age of CrA members reported in Knacke et al. (1973) and Wilking et al. (1992), and the newly detected YSOs, using the evolutionary tracks from D’Antona & Mazzitelli (1994). For the distance, we used 130 pc provided by de Zeeuw et al. (1999) and Bertout et al. (1999), who investigated the distance of CrA in addition to Upper Sco.

We also added some YSOs, which are located in isolation or at other regions, to our target list, because they have intriguing features or they are located at nearer distance. Finally, we note that our target selections were verified by considering the observational efficiency of all SEEDS targets including YSO targets and their observability such as visibility in the allocated nights.

We adopt the age and distance of YSOs if individual observations have been conducted and use these parameters to estimate detection limit in mass unit (see Section 4.2 for details). For example, distances of YSOs in Upper Sco and CrA have been catalogued in Hipparcos (de Zeeuw et al. 1999; Bertout et al. 1999) respectively. Note that we assume and refer to the stellar parameters on Table 5 for discussions of detection limits in Section 4.3 and Section 4.2.

Table 2
YSO targets in SEEDS observations

HD name	Other name	Group	RA ^a	DEC ^a	R mag ^b	Criteria ^c
...	TYC 4496-780-1	isolated	00 13 40.5677	+77 02 10.893	9.4	$H\alpha$, FIR excess
21997	...	Columba	03 31 53.64694	-25 36 50.9366	6.3	nearby, Tr-like disk
...	LkH α 330	Perseus	03 45 48.28	+32 24 11.9	11.2	Tr-disk, gap
...	IRAS 04028+2948	Taurus-Auriga	04 05 59.624	+29 56 38.26	12.3	IR excess

Table 1
Adopted age and distance of target star-forming groups.

Group	Age [Myr]	Distance [pc]	reference
Upper Scorpius (Upper Sco)	9–13	145	de Zeeuw et al. (1999) Bertout et al. (1999) Pecaut et al. (2012)
Taurus-Auriga	1–13	140	Bertout et al. (2007) Kenyon et al. (2008) Küçük & Akkaya (2010)
Ophiuchus	0.3–3	120	Greene & Meyer (1995) Lombardi et al. (2008)
Lupus	0.1–10	155	Hughes et al. (1993) Hughes et al. (1994) Lombardi et al. (2008)
Corona Australis (CrA)	0.5–10	130	Bertout et al. (1999) de Zeeuw et al. (1999) Neuhäuser et al. (2000)

Table 2 — Continued

HD name	Other name	Group	RA ^a	DEC ^a	<i>R</i> mag ^b	Criteria ^c
...	IRAS 04125+2902	Taurus-Auriga	04 15 42.787	+29 09 59.77	14.0	Tr-disk
...	LkCa 4, V1068 Tau	Taurus-Auriga	04 16 28.109	+28 07 35.81	11.8	class III, Li
...	Elias 1, V892 Tau	Taurus-Auriga	04 18 40.598	+28 19 15.51	14.4	circumbinary disk
281934	BP Tau	Taurus-Auriga	04 19 15.83527	+29 06 26.8927	11.6	full disk, CO depletion
...	V819 Tau	Taurus-Auriga	04 19 26.260	+28 26 14.30	11.2	class III, FIR excess, Tr-disk
283571	RY Tau	Taurus-Auriga	04 21 57.41003	+28 26 35.5709	9.7	Tr-like disk, gap
284419	T Tau	Taurus-Auriga	04 21 59.43445	+19 32 06.4182	9.8	IR excess
...	LkCa 8, IP Tau	Taurus-Auriga	04 24 57.080	+27 11 56.50	12.5	preTr-disk
...	DG Tau	Taurus-Auriga	04 27 04.698	+26 06 16.31	12.3	disk with jet
285846	UX Tau	Taurus-Auriga	04 30 03.99626	+18 13 49.4355	9.8	famous, Tr-disk
...	HL Tau	Taurus-Auriga	04 31 38.437	+18 13 57.65	14.2	multi-ring disk
...	L1551-51, V1075 Tau	Taurus-Auriga	04 32 09.269	+17 57 22.75	11.8	class III, Li
...	GG Tau(A)	Taurus-Auriga	04 32 30.346	+17 31 40.64	11.5	circumbinary disk
...	L1551-55, V1076 Tau	Taurus-Auriga	04 32 43.732	+18 02 56.33	11.6	class III, Li
...	DL Tau	Taurus-Auriga	04 33 39.062	+25 20 38.23	11.9	IR excess
...	DM Tau	Taurus-Auriga	04 33 48.718	+18 10 09.99	13.4	Tr-disk
...	CI Tau	Taurus-Auriga	04 33 52.005	+22 50 30.18	12.3	full disk, IR excess
...	DN Tau	Taurus-Auriga	04 35 27.375	+24 14 58.93	11.8	IR excess
...	LkCa 14, V1115 Tau	Taurus-Auriga	04 36 19.093	+25 42 59.08	10.8	class III, Tr-like disk
...	LkCa 15, V10759 Tau	Taurus-Auriga	04 39 17.796	+22 21 03.48	11.6	Tr-disk
...	LkH α 332/G1, V1000 Tau	Taurus-Auriga	04 42 07.326	+25 23 03.23	9.9	H α , Tr-like disk
...	GO Tau	Taurus-Auriga	04 43 03.095	+25 20 18.75	14.3	Tr-like disk
...	GM Aur	Taurus-Auriga	04 55 10.983	+30 21 59.54	11.7	Tr-disk
282630	LkCa 19	Taurus-Auriga	04 55 36.961	+30 17 55.19	10.6	class III, Tr-like disk
31293	AB Aur	Taurus-Auriga	04 55 45.84521	+30 33 04.2867	7.0	famous, asymmetric disk
282624	SU Aur	Taurus-Auriga	04 55 59.38527	+30 34 01.5190	9.2	IR excess, asymmetric disk
...	V397 Aur	Taurus-Auriga	04 56 02.022	+30 21 03.68	11.3	class III, Tr-like disk
...	V1207 Tau, RX J0458.7+2046	Taurus-Auriga	04 58 39.74	+20 46 44.1	11.5	Li, diskless SED
31648	MWC 480	Taurus-Auriga	04 58 46.26534	+29 50 36.97506	7.8	full disk
34282	...	ONC ^d	05 16 00.47763	-09 48 35.4169	9.8	Tr-disk
36112	MWC 758	Taurus-Auriga	05 30 27.52969	+25 19 57.0823	8.3	Tr-disk
36910	CQ Tau	Taurus-Auriga	05 35 58.46690	+24 44 54.0950	10.6	Tr-like disk
290764	V1247 Ori	ONC ^d	05 38 05.2497	-01 15 21.670	9.9	Tr-disk
...	TW Hya	TW Hya	11 01 51.90671	-34 42 17.0323	10.4	famous, nearby, Tr-disk
...	PDS 70	Centaurus	14 08 10.15	-41 23 52.5	11.3	Tr-disk
135344B	SAO 206462	Lupus	15 15 48.4394	-37 09 16.026	8.7	Tr-disk, gap
139614	...	Lupus-Ophiuchus	15 40 46.3816	-42 29 53.548	8.2	preTr-disk
...	GQ Lup	Lupus	15 49 12.102	-35 39 05.12	11.0	companion
141441	HIP 77545	Upper Sco	15 49 59.78565	-25 09 03.559315	9.0	IR excess
142315	HIP 77911	Upper Sco	15 54 41.59596	-22 45 58.5086	6.8	debris disk
...	IM Lup	Lupus	15 56 09.17658	-37 56 06.1193	13.4	full disk
142527	HIP 78092	Lupus	15 56 41.88986	-42 19 23.2746	8.3	famous, asymmetric disk, gap
...	RX J1603.9-2031A	Upper Sco	16 03 57.677	-20 31 05.51	11.7	IR excess
...	RX J1604.3-2130A, USco J1604	Upper Sco	16 04 21.66	-21 30 28.4	11.8	Tr-disk
...	SZ 91	Lupus	16 07 11.592	-39 03 47.54	14.1	Tr-disk
144587	HIP 78996	Upper Sco	16 07 29.92514	-23 57 02.4498	9.1	debris disk
...	V1094 Sco, RX J1608.6-3922	Lupus	16 08 36.183	-39 23 02.51	12.5	Tr-disk
145655	HIP 79462	Upper Sco	16 12 55.33509	-23 19 45.7022	9.0	debris disk
147137	HIP 80088	Upper Sco	16 20 50.23268	-22 35 38.7985	9.0	debris disk
...	IRAS 16225-2607, V896 Sco	Ophiuchus	16 25 38.492	-26 13 54.08	10.8	Tr-like disk
...	DoAr 25	Ophiuchus	16 26 23.678	-24 43 13.86	12.7	(less-evolved) Tr-disk
148040	HIP 80535	Upper Sco	16 26 29.91023	-27 41 20.2520	8.3	IR excess
...	DoAr 28	Ophiuchus	16 26 47.42	-23 14 52.2	12.1	Tr-disk
...	SR 21	Ophiuchus	16 27 10.278	-24 19 12.74	13.2	Tr-disk, gap

Table 2 — Continued

HD name	Other name	Group	RA ^a	DEC ^a	R mag ^b	Criteria ^c
...	IRAS 16245-2423, Oph IRS 48	Ophiuchus	16 27 37.190	-24 30 35.03	16.7	Tr-disk
...	ROXs 42B	Ophiuchus	16 31 15.016	-24 32 43.70	13.0	companion
...	DoAr 44, ROX 44	Ophiuchus	16 31 33.46	-24 27 37.3	11.7	preTr-disk
...	RX J1633.9-2442	Ophiuchus	16 33 55.61	-24 42 05.0	14.1	Tr-disk
169142	...	isolated	18 24 29.7787	-29 46 49.371	8.2	gap, companion candidate
...	MWC 297	Serpens-Aquila	18 27 39.527	-03 49 52.05	11.3	Tr-disk
...	RX J1842.9-3532	CrA	18 42 57.948	-35 32 42.69	11.6	Tr-disk
...	RX J1852.3-3700	CrA	18 52 17.299	-37 00 11.95	11.8	Tr-disk
179218	...	isolated	19 11 11.25432	+15 47 15.6388	7.3	IR excess, resolved disk
200775	HIP 103763	Cepheus	21 01 36.91964	+68 09 47.7639	8.7	flared disk

^a Values of right ascension and declination taken from Hog et al. (1998), Høg et al. (2000), Cutri et al. (2003), Zacharias et al. (2003), Zacharias et al. (2005), and van Leeuwen (2007).

^b R-band magnitudes taken from our photometric measurements, the UCAC 4 (Zacharias et al. 2012), and the USNO-B1.0 catalog (Monet et al. 2003).

^c Motivations of target selections, whose details and references are described in Section 4.3.

^d Orion Nebula Cluster

3. OBSERVATIONS AND DATA REDUCTION

SEEDS observed about 70 YSOs (more than 100 data sets in total) from 2009 October to 2015 December. SEEDS has adopted polarization differential imaging (PDI; Kuhn et al. 2001) technique together with angular differential imaging (ADI; Marois et al. 2006) in order to efficiently observe both exoplanets and circumstellar disks around those YSO targets. The PDI uses polarization and is useful to image circumstellar disks, since the scattered light from disk surfaces tends to be polarized. Using PDI, SEEDS has mainly reported the results of disk observations for YSOs. However, this technique is not suitable to the exoplanet detections, because self-luminous exoplanets at wide orbits are basically unpolarized. Meanwhile, the ADI takes advantages of field rotation to remove stellar halo and speckles. This method is the most sensitive way to find such a self-luminous exoplanet, since it does not make use of polarization, and can be applied to a detection of point source. Our YSO observations were conducted using the ADI and PDI techniques simultaneously to search for planets and analyze disks with the identical data set. Thus, ordinary and extra-ordinary rays are simultaneously obtained by dividing one frame into two or four sub-frames. However, note that our data reductions detailed in Section 3.2.1 combine all sub-frames in each frame, so the polarization information is not used in the PSF subtractions and only the ADI PSF subtractions are applied to data reductions. We here explain the observations and data reductions to search for exoplanet around the SEEDS/YSO targets.

3.1. SEEDS Observations

Table 3 lists employed filters, imaging modes and observation dates for each target. As shown in Table 3, we have observed some targets at multiple nights, for following up detected companion candidates (CCs), characterizing disks, and compensating for previous poor-quality observations. In order to test whether the CCs are physically associated with their primary stars, we need to confirm that the CCs share the common proper motions (CPMs) with the primary stars.

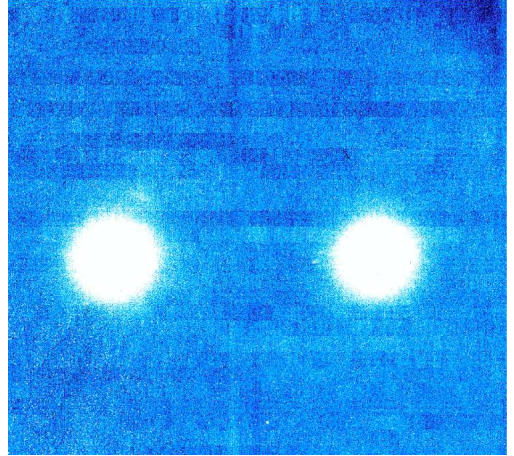


Figure 1. A Subaru/HiCIAO raw image taken in sPDI+ADI mode.

Our direct imaging observations were conducted using the adaptive optics system AO188 (Hayano et al. 2008) on the Subaru Telescope. All but 3 YSOs have been observed using them as the natural guide stars (NGSs) for AO188. However, IRS 04125+2902, IRAS 16245-2423 and RX J1633.9-2422 are too faint to be observed with the NGS mode, and we accordingly chose the laser guide star mode for those faint targets.

The near-infrared camera HiCIAO (Suzuki et al. 2010) was used simultaneously with AO188. Then, multiple differential-imaging modes are available; we can use the ‘standard PDI’ (sPDI) and ‘quad PDI’ (qPDI) modes besides the standard ADI mode. We explain all of modes below.

Subaru/HiCIAO adopts sPDI where we can get ordinary and extra-ordinary rays simultaneously with one Wollaston prism and qPDI where we can get two ordinary and extra-ordinary rays simultaneously with 2 Wollaston prisms. Therefore sPDI show 2 images in one frame and qPDI show 4 images in one frame (see Figure 1 and 2). HiCIAO PDI observations set an angular offset to decrease instrumental effects of polarization.

The field of views (FOVs) are $\sim 20'' \times \sim 20''$, $\sim 20'' \times \sim 10''$ (or $\sim 10'' \times \sim 20''$ before 2014 April), and $\sim 5'' \times \sim 5''$ for the ADI, sPDI, and qPDI modes, respectively (see Figure 1 and 2). We found that the new FoV configuration of sPDI can improve the PSF subtractions. Our observations were basically performed using an H-band ($\sim 1.6 \mu\text{m}$) filter, but a K_s-band ($\sim 2.2 \mu\text{m}$) filter was used in the case of follow-up observations or bad-seeing conditions.

We explore a faint companion around a YSO by ac-

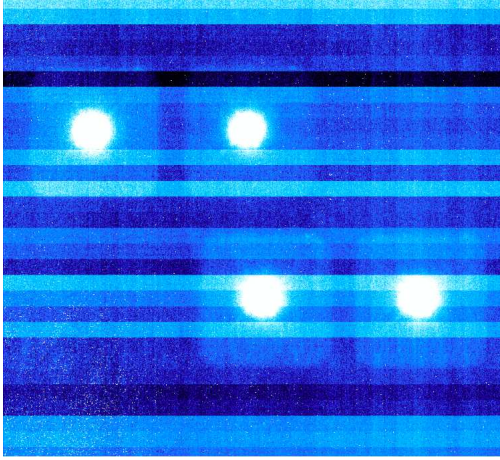


Figure 2. A Subaru/HiCIAO raw image taken in qPDI+ADI mode.

quiring deep long-integration images. While a part of our YSO targets is faint enough to be observable without saturating their images, the point spread functions (PSFs) of bright targets were weakly saturated to increase the integration times. In addition, we observed some YSOs using occulting masks, helping us avoid excessive saturation and increase integration times. Table 3 lists the targets observed with occulting masks and the mask sizes.

In addition to the saturated frames, we took unsaturated and unmasked frames for a YSO target using neutral density (ND) filters with transmittance of 9.74% at H (10.5% at K_s), 0.854% at H (1.14% at K_s), or 0.063% at H (0.138% at K_s). These are used to verify the centroid measurements for the masked or saturated images of central star (see Section 3.2). Also, these frames are used to measure the contrast between a detected companion and the primary star.

The images of globular cluster M5 or M15 were obtained in the HiCIAO runs, and are compared with archival data from *Hubble Space Telescope* to measure the field distortion, including the plate scale and offset angle between the detector’s vertical axis and the celestial north direction.

We measured the HiCIAO’s plate scales, which depend on the optical configurations (Brandt et al. 2013) and range from ~ 9.46 to ~ 9.68 mas pixel $^{-1}$ along X axis and ~ 9.77 to ~ 10.02 mas pixel $^{-1}$ along Y axis. While the pixel scales vary along the X- and Y-axes, the aspect ratio has been extremely stable. Furthermore, the orientation angles between the HiCIAO’s vertical axis and celestial north have been stably fixed to $\sim 0^\circ.3$ – $0^\circ.2$. These measurements are proper to the HiCIAO’s (ADI+)sPDI or qPDI modes, though the almost same results have been obtained by analyzing the globular cluster data taken in the ADI mode alone (Brandt et al. 2013). After the distortion correction, the plate scale is corrected to be 9.5 mas pixel $^{-1}$ and the orientation angle is corrected to be zero.

Table 3
SEEDS/YSO Observing logs

HD name	Other name	t_{tot} [min]	Rotation angle [deg]	Band	Mode	Date (HST)
...	TYC 4496-780-1	54	41.7	H	qPDI+ADI	2012 Jul 10
21997	...	36	13.8	H	sPDI+ADI+0''.4mask	2013 Jan 3
...	LkH α 330	27	10.2	H	sPDI+ADI+0''.4mask	2011 Dec 22
		22	37.3	H	qPDI+ADI	2014 Oct 9
		24	52.1	K_s	qPDI+ADI	2015 Jan 11
...	IRAS 04028+2948	45	31.5	H	qPDI+ADI	2012 Dec 31
...	IRAS 04125+2902	24	15.4	H	sPDI+ADI	2013 Nov 24
		17	9.1	H	sPDI+ADI	2014 Jan 20
...	LkCa 4, V1068 Tau	23	26.1	H	qPDI+ADI	2012 Nov 3
...	Elias 1, V892 Tau	24	5.3	H	sPDI+ADI+0''.4mask	2013 Feb 26
281934	BP Tau	32	15.5	H	qPDI+ADI	2012 Sep 13
...	V819 Tau	33	12.8	H	qPDI+ADI	2012 Jan 1
283571	RY Tau	6	89.2	H	sPDI+ADI+0''.4mask	2011 Jan 27
		19	77.2	H	sPDI+ADI	2014 Oct 6
284419	T Tau	12	1.6	H	qPDI+ADI	2015 Jan 8
...	LkCa 8, IP Tau	31	29.2	H	qPDI+ADI	2011 Dec 30
...	DG Tau	26	6.1	H	qPDI+ADI	2015 Jan 11
285846	UX Tau	30	8.9	H	qPDI+ADI	2013 Nov 24
...	HL Tau	40	3.6	K_s	qPDI+ADI	2015 Jan 8
...	L1551-51, V1075 Tau	26	1.8	H	qPDI+ADI	2012 Nov 4
...	GG Tau(A)	33	0.9	H	sPDI+ADI+0''.6mask	2011 Sep 4
...	L1551-55, V1076 Tau	26	2.5	H	qPDI+ADI	2012 Nov 5
...	DL Tau	30	72.3	K_s	qPDI+ADI	2014 Oct 6
...	DM Tau	12	162.1	H	sPDI+ADI	2009 Dec 23
...	CI Tau	32	130.4	H	qPDI+ADI	2012 Sep 13
...	DN Tau	12	161.4	H	sPDI+ADI	2009 Dec 22
...	LkCa 14, V1115 Tau	28	27.0	H	sPDI+ADI	2011 Dec 29
...	LkCa 15, V1079 Tau	11	134.8	H	sPDI+ADI	2009 Dec 25
		11	10.6	H	ADI	2010 Jan 22
		40	4.5	K_s	sPDI+ADI	2010 Dec 1
		5	11.5	K_s	sPDI+ADI	2011 Jan 27
		34	4.4	H	qPDI+ADI	2013 Nov 12
...	LkH α 332/G1, V1000 Tau	28	4.0	H	sPDI+ADI+0''.4mask	2013 Jan 3
...	GO Tau	40	16.7	H	sPDI+ADI	2009 Dec 24
...	GM Aur	12	31.8	H	qPDI+ADI	2010 Dec 2

Table 3 — Continued

HD name	Other name	t_{tot} [min]	Rotation angle [deg]	Band	Mode	Date (HST)
282630	LkCa 19	22	100.7	<i>H</i>	sPDI+ADI	2011 Dec 22
		31	51.1	<i>H</i>	sPDI+ADI	2011 Dec 23
31293	AB Aur	8	50.1	K_s	sPDI+ADI	2009 Dec 24
282624	SU Aur	24	14.3	<i>H</i>	qPDI+ADI	2014 Jan 19
		13	47.9	K_s	qPDI+ADI	2014 Oct 9
...	V397 Aur	23	75.2	<i>H</i>	sPDI+ADI	2011 Dec 31
...	V1207 Tau, RX J0458.7+2046	17	125.0	<i>H</i>	qPDI+ADI	2012 Nov 3
		20	57.6	<i>H</i>	sPDI+ADI	2015 Dec 28
31648	MWC 480	52	69.9	<i>H</i>	sPDI+ADI	2010 Jan 24
34282	...	38	11.5	<i>H</i>	sPDI+ADI+0''4mask	2011 Dec 29
36112	MWC 758	25	6.9	<i>H</i>	sPDI+ADI+0''4mask	2011 Dec 23
		17	14.3	K_s	qPDI+ADI	2011 Dec 25
		30	102.1	<i>H</i>	qPDI+ADI	2013 Oct 16
36910	CQ Tau	30	2.1	<i>H</i>	sPDI+ADI	2012 Jan 1
		28	4.0	<i>H</i>	sPDI+ADI+0''3mask	2014 Oct 11
		9	3.2	<i>H</i>	sPDI+ADI	2015 Dec 30
290764	V1247 Ori	42	31.7	<i>H</i>	sPDI+ADI+0''3mask	2013 Nov 23
		36	29.9	<i>H</i>	qPDI+ADI	2014 Jan 19
		30	35.2	K_s	ADI	2015 Jan 7
...	TW Hya	23	13.3	<i>H</i>	qPDI+ADI	2011 Mar 25
		30	12.2	<i>H</i>	qPDI+ADI	2013 Jan 3
...	PDS 70	23	24.1	<i>H</i>	qPDI+ADI	2012 Feb 27
135344B	SAO 206462	18	23.4	<i>H</i>	sPDI+ADI+0''4mask	2011 May 20
139614	...	26	15.2	<i>H</i>	sPDI+ADI+0''4mask	2014 Jun 6
...	GQ Lup	30	16.1	<i>H</i>	qPDI+ADI	2013 May 17
		48	14.3	<i>H</i>	sPDI+ADI+0''4mask	2013 May 19
141441	HIP 77545	31	34.6	<i>H</i>	sPDI+ADI	2012 May 12
		25	14.7	<i>H</i>	ADI	2014 Jun 7
142315	HIP 77911	32	28.2	<i>H</i>	sPDI+ADI	2012 May 10
		20	10.5	<i>H</i>	ADI	2014 Jun 8
...	IM Lup	28	17.7	<i>H</i>	qPDI+ADI	2014 Jun 7
142527	HIP 78092	14	19.3	K_s	sPDI+ADI+0''4mask	2011 May 25
		12	20.4	<i>H</i>	sPDI+ADI	2012 Apr 10
...	RX J1603.9-2031A	52	22.9	<i>H</i>	qPDI+ADI	2012 Jul 9
...	RX J1604.3-2130A, USco J1604	25	10.3	<i>H</i>	qPDI+ADI	2012 Apr 11
...	SZ 91	44	42.7	K_s	sPDI+ADI	2012 May 10
144587	HIP 78996	34	29.8	<i>H</i>	sPDI+ADI+0''4mask	2011 May 24
		10	3.9	<i>H</i>	sPDI+ADI	2013 May 17
...	V1094 Sco, RX J1608.6-3922	36	21.2	<i>H</i>	sPDI+ADI+0''4mask	2011 May 20
145655	HIP 79462	40	12.8	<i>H</i>	ADI	2012 Apr 11
		27	14.8	<i>H</i>	ADI	2014 Apr 22
		32	25.3	<i>H</i>	ADI	2015 Apr 29
147137	HIP 80088	10	5.7	<i>H</i>	ADI	2012 Jul 5
		37	16.6	<i>H</i>	sPDI+ADI	2012 Jul 10
...	IRAS 16225-2607, V896 Sco	29	32.0	<i>H</i>	qPDI+ADI	2012 May 11
...	DoAr 25	33	25.3	<i>H</i>	qPDI+ADI	2012 May 15
		11	7.2	<i>H</i>	ADI	2014 Jun 9
148040	HIP 80535	40	36.6	<i>H</i>	sPDI+ADI	2012 May 13
		10	8.5	<i>H</i>	ADI	2015 Apr 29
...	DoAr 28	48	30.5	<i>H</i>	qPDI+ADI	2012 Jul 8
		32	22.2	<i>H</i>	qPDI+ADI	2014 Jun 8
...	SR 21	18	10.7	<i>H</i>	qPDI+ADI	2011 May 22
...	IRAS 16245-2423, Oph IRS 48	28	14.3	<i>H</i>	qPDI+ADI	2013 May 19
...	ROXs 42B	15	11.7	<i>Y</i>	ADI	2014 Jun 8
...	DoAr 44, ROX 44	30	26.7	<i>H</i>	qPDI+ADI	2011 May 22
		6	4.4	K_s	sPDI+ADI	2012 May 12
...	RX J1633.9-2442	46	22.8	<i>H</i>	qPDI+ADI	2014 Apr 23
169142	...	40	23.1	<i>H</i>	sPDI+ADI+0''4mask	2011 May 23
		30	13.2	<i>J</i>	sPDI+ADI+0''4mask	2013 May 19
...	MWC 297	20	36.2	<i>H</i>	sPDI+ADI	2012 Jul 7
...	RX J1842.9-3532	34	13.8	<i>H</i>	qPDI+ADI	2012 Sep 13
...	RX J1852.3-3700	33	29.2	<i>H</i>	sPDI+ADI	2011 Sep 5
179218	...	34	2.3	<i>H</i>	sPDI+ADI+0''4mask	2012 Sep 12
200775	HIP 103763	28	26.5	<i>H</i>	sPDI+ADI+0''4mask	2011 Sep 4

3.2. Data Reduction

3.2.1. ADI Data Reductions

Our YSO targets have been observed using PDI+ADI mode. The data reduction pipelines previously used

to search for exoplanets (e.g., Kuzuhara et al. 2013; Brandt et al. 2013) are dedicated to the data obtained with only ADI technique. To reduce the ADI+PDI data, we have customized an IDL pipeline for ADI reductions, and developed some auxiliary routines that are based on Python and PyRAF.

For sPDI+ADI or qPDI+ADI data, we first remove

their correlated read noise (i.e., destriping), correct for hot pixels, and perform flat-fielding, similarly as for standard SEEDS ADI data (e.g., Brandt et al. 2013). After these processes, each frame is divided into 2 and 4 sub-frames in the case of sPDI and qPDI observations, respectively. In the sPDI+ADI mode, each sub-frame contains either ordinary ray or extra-ordinary ray for a YSO target. Meanwhile, in the qPDI+ADI mode, the four sub-frames contains two ordinary and extra-ordinary rays. The centroids of target on each sub-frame are individually estimated and each image for the target is shifted to a common center, after correcting field distortion of all sub-frames; the distortion-corrected plate scale is 9.5 mas pixel⁻¹. We subsequently integrate the sub-images that were simultaneously acquired into a single image. Finally, the ADI reductions are applied to the sequence of images made by integrating each simultaneous image. When measuring a detected object’s celestial coordinate relative to its central star, we corrected the artificial angular offset in our PDI observations (see Section 3.1).

In order to estimate the stellar centroids, we take into account the three different methods explained below. The first method is applied to a target observed with the long sequence of unsaturated data, for which we calculate the center of a PSF by fitting a 2-dimension elliptical Gaussian function to the PSF on each image with IRAF. The second method is applied to saturated data. Then, we choose a reference frame from all saturated frames for a target, and calculate the relative centroids by comparing the reference frame with the rest of saturated frames. As in Section 3.1, we obtained unsaturated frames for a YSO target, in the same night. The unsaturated frames are used to verify the centroid of reference frame.

For masked data, we adopt the third method, which estimates a position of star by fitting a Moffat function to its masked PSF. In the fit, we exclude the masked area of PSF. Moffat function is given as:

$$I(r) = I_0 \left[1 + \left(2 \frac{\sqrt{(x - x_c)^2 + (y - y_c)^2}}{W} \right)^2 \right]^\beta, \quad (1)$$

where I_0 is the peak value of PSF, x_c and y_c are the x and y center of PSF, W is FWHM, and β is atmosphere scattering coefficient (Moffat 1969). Using least-square fit, each parameter in Equation (1), including x_c and y_c , is determined. This method based on Moffat function fit should be the best way to determine a center of image whose PSF core is largely masked (0'3–0'4 in our observations; Walker et al. 1994).

The AO188 keeps target’s centroids stable during observations. Furthermore, atmospheric dispersion corrector (ADC; Egner et al. 2010) in AO188 is available to help mitigate the drift of centroids. Typically, centroid drifts are less than 1–2 pixels (~ 10 – 20 mas) over long sequence of integrations for each target (Brandt et al. 2013). Even in observations at high airmass (Thalmann et al. 2011), the centroid drift is no more than a few tens of mas (Brandt et al. 2013). The image-registration algorithms explained above can remove the remaining centroid drifts that are not corrected by AO188; a drift is typically found to be less than ~ 10 mas.

In order to improve the sensitivities of our observations, it is crucial to acquire as long integrations as possible. However, a central star’s PSF is usually made more saturated as the integration time of an individual frame increases. We note the balance between a PSF saturation and an integration time. After subtracting a radial profile from each intensity image, we perform ADI-LOCI data processing (Lafreniere et al. 2007) to attenuate starlight and speckles. LOCI requires to tune some parameters, which affect the performance of data reductions. At a radial distance ($= R$) from each central star, our LOCI processing requires a minimum field rotation of $0.75 (= N_\delta) \times \text{PSF's FWHM} / R$ radian between a PSF-subtracted image and the PSF-reference images. Our software masks the regions that do not have field rotations large enough to pass this criterion. In addition, an optimization zone for reference-PSF modeling has an area of $300 (= N_A) \times \pi(\text{FWHM}/2)^2$ pixels. See Lafreniere et al. (2007) for details of LOCI parameters. All the LOCI-processed frames are median-combined into a final high-SN image.

LOCI partially decreases a flux of point source due to self-subtractions of its PSFs. This flux loss is more significant at smaller separations (Lafreniere et al. 2007). We estimate the artificial flux loss applying LOCI to the data with injected fake companions. We initially inject the fake sources with SN ratios of ~ 15 , from $\sim 0''.2$ to the edge of the FOV. This procedure is repeated 15 times changing initial position angle to cover the full range of (r, θ) in the field avoiding the overlap of PSFs. Finally, we measure the flux loss at each position of more than 1000 fake companions and plot the radial profile of self-subtraction. As to SEEDS data, the typical flux loss is $\sim 50\%$ at $0''.3$, $\sim 20\%$ at $0''.8$, and under 10% at larger distances than $1''$. In addition, we correct the flux loss to derive the photometry of detected companion and contrast limit on each target (see Section 3.2.2).

3.2.2. Producing Contrast Curves

Discussion about exoplanet frequency based on statistical analysis requires detection limits for each target. We calculate the detection limit by defining a noise distribution. First, the final reduced image for each target is normalized by dividing the image by its integration time. Next, the normalized map is convolved with an aperture, whose radius is equal to half of the central star PSF’s FWHM. An aperture of the same size was used for the photometry of the central star in unsaturated frames. Finally, we define the rings at intervals of $\sim 0''.06$ from the central stars and measure the standard deviation of counts at each ring in the convolved map. The standard deviations are determined to be the noises as a function of angular separations from the central star. To produce a contrast curve, the noise function is divided by the flux of the central star’s unsaturated PSFs. Some SEEDS/YSO observations in the early part took reference frames with occulting masks or did not take unsaturated frames. These observations have disadvantages in that we have to use other observations for photometric reference, which increases the uncertainty of the contrasts. The partial flux losses in the contrast curves have been corrected. Finally, we adopt 5σ detection threshold in this paper.

Sensitivity and contrast depend on weather condition,

AO performance (seeing), and integration time. Some data were taken in bad condition whose detection limit was not good and are not meaningful for the exoplanet survey due to low contrast. We note that accurately estimating the flux loss by self-subtraction at small angular separations is a difficult task.

4. RESULTS

Among our whole observations, a few observations were conducted with only PDI that cannot be used for exoplanet search. Excluding these, we finally reduced the data taken for the 68 YSO targets (99 data sets in total) to explore planetary-mass companion candidate. Note that some data have the rotation angles that are too small to explore inner (< 100 AU) region. We do not include sources with signal-to-noise ratios (SNRs) less than 5 in the list of companion candidates. As a result, we found 15 new companion candidates within 400 AU from their central stars. We detected a new stellar companion physically associated with HIP 79462 (see Section 4.3.52). We also detected an unreported bright source around TYC 4496-780-1 (see Section 4.3.1) which is either a stellar companion or a background star. In addition, we confirmed 2 convincing low-mass companions. These companions have been reported previously; GQ Lup b (see Section 4.3.42) and ROXs 42B b (see Section 4.3.60).

Although our observations detected more point sources, it is impossible to statistically explore the objects at the projected separations larger than 400 AU because a lot of targets have been observed with qPDI, which has a FOV corresponding to 400 AU. Moreover, we assume that planet formations at such large separations from primary stars are relatively challenging since the standard disks around pre-main sequence star should not be so large (c.f. Andrews & Williams 2007), less prioritizing the follow-up observations of those wide-separation companions. Note that there are the existences of substellar companions at the very large distances from their primary stars (e.g. Bailey et al. 2014; Naud et al. 2014). With the caveat that such substellar companions with very wide separations cannot be ruled out as the companions formed from the circumstellar disks, we do not discuss the companion candidates at the separations larger than 400 AU, based on the above reasons. The 7 point sources out of 15 candidates within 400 AU from their central stars are identified to be background stars by conducting common proper motion test.

We present the detailed frameworks of detection limits and luminosity-mass conversion in Section 4.1 and 4.2. We also summarize our observed results for individual targets.

4.1. Contrast

Our results of detection limit are listed in Table 4. Note that SEEDS observations are carried out basically in H -band, but some YSOs are observed in only K_s -

band. For the YSOs observed at multiple epochs, we adopt the deepest detection limits among all detection limits from multiple observations. Figures 9 and 10 show our final results of 5σ detection limit with bright (< 8 mag in H or K_s -band) and faint (≥ 8 mag) stars. Sources brighter than contrast curves can be detected by HiCIAO observations with more than 5σ significance. Comparing Figures 9 with 10, we find that typical detection limits are better in observing bright YSOs by a factor of ~ 2 – 10 than faint YSOs. We calculated the typical limiting magnitudes by adding the brightness of central stars to the contrast curves, in order to investigate whether or not this difference arises from the difference of AO efficiency. As a result, the limiting magnitudes around bright and faint targets are almost the same; ~ 14 – 15 mag at $0''.3$, ~ 15.5 – 17 mag at $0''.5$, ~ 18 – 19 mag at $1''.0$, ~ 19 – 20 mag beyond $2''.0$.

As already described in Section 3.2.2, some of early observations did not take unsaturated frames, thus we need to use the data of the other targets as photometric reference, making it more uncertain to estimate the contrast limits. Actually, a bundle of contrast curves in Figure 9 and 10 look wider than those by Moving Group targets (Brandt et al. 2014b,a) to some extent. In CQ Tau, GQ Lup, HIP 103763, HIP 79462, IRAS 16225-2607, MWC 297, PDS 70, ROX44, TYC 4496-780-1 and UX Tau data, there are bright point sources affecting contrast curves. We masked these bright sources when deriving detection limits but we cannot completely remove their influences on detection. IRAS 04125+2902 and LkHa 332 G1 also have bright sources in the FOV, but the companions are outside of our explored separation range. We typically achieve contrast of $\sim 10^{-3.5}$ at $0''.5$, 10^{-4} – 10^{-5} at $1''$ and $10^{-4.5}$ – 10^{-6} beyond $2''$. This detection limit is similar to that of other SEEDS categories (Brandt et al. 2014b) and one of the highest contrasts among the YSO imaging surveys conducted so far (see Section 5.3.2). There are a lot of bad pixels at the edges of detector which can affect the contrast curves, and some contrast curves actually become shallower at the wider separations.

Figure 11 compares the detection limits of this work with some of previous high contrast surveys. Note that some previous works set detection significances different from 5σ and adopted different filters in imaging observations. In comparison with the results of other high contrast imaging surveys for young moving groups (see Section 5.3.1), our median contrast limits appear to be lower at $1''$. YSOs are basically located at farther distances and thus fainter than young moving group members, affecting AO performance. Nevertheless, although our results of contrast looks shallow in terms of contrast, the central stars are generally faint so our data can be as deep as those of the other previous studies in terms of limiting magnitude. Eventually, planets around YSOs are younger and brighter than those in the young moving groups, enabling us to constrain a few times higher than jovian mass. On the other hand, our survey achieved the strongest constraints compared to other YSO imaging surveys (see Section 5.3.2).

Table 4
SEEDS/YSO detection limits

HD name	Other name	Magnitude (band) ^a	Δ mag (5σ contrast)						
			0''25	0''5	0''75	1''0	1''5	2''0	3''0
...	TYC 4496-780-1	7.76±0.02 (<i>H</i>)	6.2	8.8	10.1	11.1	...	11.9	10.1
21997	...	6.12±0.03 (<i>H</i>)	...	7.2	9.1	10.4	12.0	12.7	12.9
...	LkH α 330	7.92±0.03 (<i>H</i>)	...	8.8	9.9	11.2	12.4	13.1	13.1
...	IRAS 04028+2948	9.47±0.03 (<i>H</i>)	3.9	5.5	6.3	7.1	7.6	7.6	6.1
...	IRAS 04125+2902	9.76±0.03 (<i>H</i>)	...	6.3	7.8	8.5	10.1	10.6	10.8
...	LkCa 4, V1068 Tau	8.52±0.02 (<i>H</i>)	...	8.9	10.0	11.1	12.1	12.4	12.5
...	Elias 1, V892 Tau	7.02±0.03 (<i>H</i>)	9.7	10.6	11.5
281934	BP Tau	8.22±0.02 (<i>H</i>)	...	8.2	9.5	10.4	11.4	11.7	8.8
...	V819 Tau	8.65±0.02 (<i>H</i>)	8.3	9.4	10.7	11.3	11.0
283571	RY Tau	6.13±0.06 (<i>H</i>)	...	8.3	10.1	11.4	13.5	14.6	15.6
284419	T Tau	6.24±0.02 (<i>H</i>)	8.3
...	LkCa 8, IP Tau	8.89±0.02 (<i>H</i>)	...	7.8	8.7	10.1	11.0	11.1	10.8
...	DG Tau	7.72±0.03 (<i>H</i>)	8.5	9.5	10.9	11.5	8.2
285846	UX Tau	7.96±0.02 (<i>H</i>)	7.5
...	HL Tau	7.41±0.02 (<i>K_s</i>)	7.3	4.6
...	L1551-51, V1075 Tau	9.06±0.02 (<i>H</i>)	8.8	9.9	10.9	11.2	11.4	11.4	9.7
...	GG Tau(A)	7.82±0.03 (<i>H</i>)	12.1
...	L1551-55, V1076 Tau	9.46±0.03 (<i>H</i>)	8.1	9.6	10.2	10.9	11.0	11.0	9.1
...	DL Tau	7.96±0.02 (<i>K_s</i>)	6.9	8.9	9.6	10.1	10.7	10.8	9.2
...	DM Tau	9.76±0.02 (<i>H</i>)	5.0	7.8	8.4	9.4	10.3	10.6	11.0
...	CI Tau	8.43±0.04 (<i>H</i>)	6.4	8.6	9.7	10.4	11.2	11.2	10.1
...	DN Tau	8.34±0.03 (<i>H</i>)	6.8	9.4	10.1	11.0	11.4	11.5	11.5
...	LkCa 14, V1115 Tau	8.71±0.03 (<i>H</i>)	...	8.6	9.7	10.8	11.8	12.1	12.2
...	LkCa 15, V1079 Tau	8.60±0.02 (<i>H</i>)	5.7	7.8	8.5	9.3	9.3	9.4	9.3
...	LkH α 332/G1, V1000 Tau	8.40±0.02 (<i>H</i>)	9.3	10.2	11.3	12.0	12.2
...	GO Tau	9.78±0.02 (<i>H</i>)	4.3	6.1	6.5	7.3	8.4	8.6	8.8
...	GM Aur	8.60±0.02 (<i>H</i>)	7.8	10.5	11.0	11.5	11.8	11.4	11.1
282630	LkCa 19	8.32±0.02 (<i>H</i>)	6.4	9.4	10.6	11.3	12.0	12.1	12.1
31293	AB Aur	4.23±0.02 (<i>K_s</i>)	6.7	8.6	9.3	9.4	10.0	10.3	10.4
282624	SU Aur	6.56±0.02 (<i>H</i>)	...	11.1	12.2	13.0	14.1	14.3	12.0
...	V397 Aur	8.32±0.02 (<i>H</i>)	6.0	8.5	9.5	10.6	11.2	11.4	11.3
...	V1207 Tau, RX J0458.7+2046	8.96±0.02 (<i>H</i>)	6.7	9.0	10.3	10.9	11.8	11.9	11.9
31648	MWC 480	6.26±0.03 (<i>H</i>)	8.0	10.9	12.5	13.6	14.8	15.1	15.1
34282	...	8.48±0.03 (<i>H</i>)	...	8.5	9.7	10.8	12.0	12.3	12.4
36112	MWC 758	6.56±0.02 (<i>H</i>)	...	9.7	11.1	11.8	13.2	13.3	10.9
36910	CQ Tau	7.06±0.02 (<i>H</i>)	11.5	13.2	13.8	14.1
290764	V1247 Ori	8.20±0.25 (<i>H</i>)	7.6	10.0	11.4	12.2	13.2	13.5	13.7
...	TW Hya	7.56±0.04 (<i>H</i>)	...	7.2	8.9	9.6	10.6	10.8	9.6
...	PDS 70	8.82±0.04 (<i>H</i>)	...	6.9	8.4	9.8	10.7	11.0	10.9
135344B	SAO 206462	6.59±0.03 (<i>H</i>)	...	8.0	9.8	11.1	12.8	13.4	13.8
139614	...	7.33±0.04 (<i>H</i>)	...	7.4	9.5	10.7	12.9	13.7	14.2
...	GQ Lup	7.70±0.03 (<i>H</i>)	...	7.9	8.9	10.0	11.0	11.4	8.8
141441	HIP 77545	8.00±0.03 (<i>H</i>)	8.7	10.4	11.8	12.8	14.2	14.5	14.7
142315	HIP 77911	6.67±0.03 (<i>H</i>)	...	9.3	10.9	11.8	13.7	14.4	14.8
...	IM Lup	8.09±0.04 (<i>H</i>)	7.3	8.7	10.1	11.1	12.3	12.2	10.0
142527	HIP 78092	5.72±0.03 (<i>H</i>)	...	10.4	12.1	12.7	14.1	14.5	14.7
...	RX J1603.9-2031A	8.77±0.03 (<i>H</i>)	...	8.7	9.7	10.8	11.4	11.4	9.6
...	RX J1604.3-2130A, USco J1604	9.10±0.02 (<i>H</i>)	7.8	9.7	10.9	11.8	12.4	12.4	11.9
...	SZ 91	9.85±0.02 (<i>K_s</i>)	...	8.5	9.3	9.6	9.6	9.8	9.8
144587	HIP 78996	7.36±0.06 (<i>H</i>)	...	9.0	10.6	11.7	12.9	13.3	13.3
...	V1094 Sco, RX J1608.6-3922	9.04±0.02 (<i>H</i>)	...	8.3	9.6	10.7	11.7	11.8	12.0
145655	HIP 79462	7.43±0.07 (<i>H</i>)	7.6	9.1	11.1	12.8	14.1	14.3	14.4
147137	HIP 80088	7.90±0.04 (<i>H</i>)	7.7	9.7	11.1	11.9	12.8	13.0	13.2
...	IRAS 16225-2607, V896 Sco	7.95±0.06 (<i>H</i>)	...	8.0	11.9	12.3	11.3	11.5	10.4
...	DoAr 25	8.40±0.05 (<i>H</i>)	...	7.3	8.4	9.4	10.8	11.3	9.9
148040	HIP 80535	7.31±0.05 (<i>H</i>)	...	8.2	9.7	11.0	12.5	13.3	13.7
...	DoAr 28	8.99±0.02 (<i>H</i>)	...	8.4	9.8	10.6	11.2	11.4	8.5
...	SR 21	7.51±0.04 (<i>H</i>)	...	9.2	10.1	11.1	12.0	12.3	10.2
...	IRAS 16245-2423, Oph IRS 48	8.82±0.07 (<i>H</i>)	...	7.6	8.5	9.4	10.6	10.7	8.2
...	DoAr 44, ROX 44	8.25±0.06 (<i>H</i>)	...	8.6	9.2	10.3	11.3	11.4	9.1
...	RX J1633.9-2442	9.36±0.02 (<i>H</i>)	...	7.8	9.2	9.7	11.1	11.2	8.5
169142	...	6.91±0.04 (<i>H</i>)	...	9.8	11.1	12.2	13.3	13.6	12.9
...	MWC 297	4.39±0.21 (<i>H</i>)	6.4	8.7	10.5	11.6	13.6	14.6	15.0
...	RX J1842.9-3532	8.71±0.04 (<i>H</i>)	...	8.0	8.8	9.6	10.9	11.2	8.3
...	RX J1852.3-3700	9.14±0.02 (<i>H</i>)	...	9.5	10.6	11.1	11.8	11.9	11.7
179218	...	6.65±0.03 (<i>H</i>)	14.1
200775	HIP 103763	5.47±0.03 (<i>H</i>)	...	9.4	11.2	12.5	13.8	12.1	11.9

^a *H*-band magnitudes taken from 2MASS (Cutri et al. 2003; Skrutskie et al. 2006).

We reveal a detected companion’s mass and how massive planets can be detected in our YSO observations. Therefore, we need to convert our 5σ contrast limit into the mass detection limit and the detected companion’s luminosity into its mass. The relationships between age, luminosity, and mass of giant planets and brown dwarfs have been theoretically modeled (e.g. Baraffe et al. 2003; Allard et al. 2011). The relations should vary depending on how planets form from circumstellar disks (Marley et al. 2007).

We adopt the age-luminosity-mass relation of COND03 model (Baraffe et al. 2003), one of hot-start models. Cold-start models have been also proposed to model the luminosity and temperature evolution of a giant planet, which depends on the planet formation scenarios (e.g., Marley et al. 2007). Observational results disagree to a very cold start model (Marleau & Cumming 2014). As mentioned in Section 1, though the controversy of formation scenario has been unsettled, the mass estimations based on the evolution models should be uncertain particularly on young exoplanets, due to the large uncertainty of the initial conditions (Marleau & Cumming 2014). To calibrate these models requires comparing parameters between estimated by direct imaging and by other methods such as radial velocity or transit. How-

ever, there are no exoplanets detected by both of direct imaging and indirect methods so far.

The luminosity-mass conversions also require the age and distance of the target, so the stellar parameters of our observed YSOs should be known in our analysis. As discussed in Section 2.2, most YSOs are located in star-forming regions, thus age and distance of YSOs can be approximately estimated from their group membership. Table 1 shows typical age and distance of star-forming regions targeted in this study. Table 5 shows the stellar parameters of each YSO. Note that we use the stellar parameters to estimate detection limits in Section 4.3 and Section 5. The individually adopted parameters are usually consistent with those of the belonging groups. CQ Tau, IM Lup, Sz 91 have somewhat different distances from the those of Taurus and Lupus. V1094 Sco, HIP 79462, USco J1604, and LkH α 332/G1 have different ages from the typical value of Upper Sco and Taurus. In this calculation, we used 10 Myr for only YSOs in Upper Sco instead of 11 Myr so as to avoid extrapolating the planet luminosity at 11 Myr from the luminosity models in 1–10 Myr. For HIP 103763 we used 1 Myr instead of the adopted age because our adopted luminosity model does not publish the calculations for the objects with such a very young age.

Table 5
Adopted Stellar Parameters of SEEDS/YSO Targets

HD name	Other name	Sp type	Av	Age [Myr]	Distance [pc]	Reference
...	TYC 4496-780-1	G ^a	...	15	150	56
21997	...	A3	...	30	72	27,29,44,66,69
...	LkH α 330	G3	1.8	3	250	22,25,65,78
...	IRAS 04028+2948	A1	...	6	140	64
...	IRAS 04125+2902	M1.25	2.39	6	140	12,37,79
...	LkCa 4, V1068 Tau	K7	1.21	2.5	140	1,13,18
...	Elias 1, V892 Tau	A6	5.93	2	140	1,18,63
281934	BP Tau	K7	0.49	2.2	140	1,18,45
...	V819 Tau	K7	1.35	2.7	140	1,18,43,68
283571	RY Tau	K1	1.84	1.1	134	1,3,5
284419	T Tau	K0	1.39	1.8	140	1,5,68
...	LkCa 8, IP Tau	M0	0.24	4.0	140	1,11,40,80
...	DG Tau	K6	1.29	9.0	140	12,68,79
285846	UX Tau	G8	0.21	1	152	1,5,6,45
...	HL Tau	K7	7.4	0.9	140	1,41,83
...	L1551-51, V1075 Tau	K7	0.0	6	140	1
...	GG Tau(A)	K7	0.76	1.5	140	1,36
...	L1551-55, V1076 Tau	K7	0.69	6	140	1
...	DL Tau	K7	1.21	1	140	3,12,17,43
...	DM Tau	M1	0.00	3.6	140	1,3
...	CI Tau	K7	1.77	1.7	140	1,3,17
...	DN Tau	M0	0.49	2.6	140	1,43
...	LkCa 14, V1115 Tau	M0	0.00	8.9	140	1,43
...	LkCa 15, V1079 Tau	K5	0.62	1.4	140	1,43
...	LkH α 332/G1, V1000 Tau	M1–M2.5	4.6	0.2	140	26,42,71
...	GO Tau	M0	1.18	4.8	140	1,3
...	GM Aur	K3–K5.5	1.2	7.2	140	3,20,84
282630	LkCa 19	K0	0.00	6	140	1
31293	AB Aur	A0–A1	0.50	3	144	2,4,45
282624	SU Aur	G2	0.90	2.2	140	1,3,45
...	V397 Aur	K7	0.00	4.4	140	1,55,68,80,86
...	V1207 Tau, RX J0458.7+2046	K7	0.3	2.7	140	52,81
31648	MWC 480	A5	0.096	6.7	146	2,31
34282	...	A3	0.16	6.4	350	2,9
36112	MWC 758	A5	0.0	3.5	279	47,49,50,66
36910	CQ Tau	F3	2.0	13	100	4,5
290764	V1247 Ori	A0/A5/F2	0.64	7.4	385	62,89
...	TW Hya	M2	0.0	8	54	57,58,66,77
...	PDS 70	K5	0.81	10	140	48,67,90,91
135344B	SAO 206462	F4	0.3	8	142	8,23,50,55,82
139614	...	A7	0.09	7.0	140	8,82,85,92
...	GQ Lup	K7–M0	1.0	3	150	15,72

Table 5 — Continued

HD name	Other name	Sp type	Av	Age [Myr]	Distance [pc]	Reference
141441	HIP 77545	A2–A3	1.25	11	119	14,66,93
142315	HIP 77911	B9	0.34	11	148	34,66
...	IM Lup	M0	0.5	1	190	19,94
142527	HIP 78092	F6	0.37	2	140	2,85,87
...	RX J1603.9-2031A	K5	0.7	11	145	73
...	RX J1604.3-2130A, USco J1604	K2	1.0	3.7	145	35,59,88
...	SZ 91	M0.5	2.0	5	200	53,72,95
144587	HIP 78996	A9	0.47	11	108	14,66,93
...	V1094 Sco, RX J1608.6-3922	K6	3.0	3	155	60,61
145655	HIP 79462	G2	0.45	6	142	14,66,93
147137	HIP 80088	A9	0.61	11	139	14,66,93
...	IRAS 16225-2607, V896 Sco	K7	1.3	0.8	120	38,39
...	DoAr 25	K5	2.7	3.8	145	20,30,97,98
148040	HIP 80535	G0	0.00	8	120	14,66,74
...	DoAr 28	K5	2.3	5	139	38,75
...	SR 21	G3	9.0	4.7	120	20,76
...	IRAS 16245-2423, Oph IRS 48	A0	12.9	1.5	120	24,38
...	ROXs 42B	M0	1.9	2.5	120	33,51
...	DoAr 44, ROX 44	K3	2.2	1.5	120	6,38,50
...	RX J1633.9-2442	K7	5.0	2.0	120	54,70
169142	...	A5	0.31	8	145	2,8,74
...	MWC 297	B1.5	8	2	250	7,46,96
...	RX J1842.9-3532	K2	1.1	5	130	21,22,37,99
...	RX J1852.3-3700	K3	1.0	5	130	21,22,37,99
179218	...	B9	0.77	1	240	10,28,32
200775	HIP 103763	B3	2.43	0.016	430	4,5,27,28

References.

- 1. Kenyon & Hartmann (1995b) 2. Fukagawa et al. (2010) 3. Ricci et al. (2010) 4. Hernández et al. (2004) 5. Bertout et al. (1999) 6. Espaillat et al. (2010) 7. Mora et al. (2001) 8. Dunkin et al. (1997) 9. Merín et al. (2004) 10. Malfait et al. (1998) 11. Gullbring et al. (1998) 12. Andrews et al. (2013) 13. White & Ghez (2001b) 14. Pecauc et al. (2012) 15. McElwain et al. (2007) 16. Neuhäuser et al. (2005) 17. Valenti et al. (1993) 18. Küçük & Akkaya (2010) 19. Pinte et al. (2008) 20. Andrews et al. (2009) 21. Silverstone et al. (2006) 22. Rigliaco et al. (2015) 23. Müller et al. (2011) 24. van der Marel et al. (2013) 25. Isella et al. (2013) 26. Herczeg & Hillenbrand (2014) 27. ESA (1997) 28. Alecian et al. (2013) 29. Moór et al. (2006) 30. Andrews et al. (2008) 31. Montesinos et al. (2009) 32. Panić & Hogerheijde (2009) 33. Bouvier & Appenzeller (1992) 34. Hernández et al. (2005) 35. Dahm & Carpenter (2009) 36. White et al. (1999) 37. Hughes et al. (2010) 38. McClure et al. (2010) 39. Rojas et al. (2008) 40. Sestito et al. (2008) 41. Kraus & Hillenbrand (2009) 42. Hartmann et al. (1998) 43. Takagi et al. (2014) 44. Torres et al. (2008) 45. Costigan et al. (2014) 46. Drew et al. (1997) 47. Benisty et al. (2015) 48. Hashimoto et al. (2012) 49. Meeus et al. (2012) 50. Andrews et al. (2011) 51. Currie et al. (2014b) 52. Wahhaj et al. (2010) 53. Tsukagoshi et al. (2014) 54. Orellana et al. (2012) 55. France et al. (2012) 56. Guillout et al. (2010) 57. Akiyama et al. (2015) 58. Herczeg et al. (2004) 59. Preibisch & Zinnecker (1999) 60. Bustamante et al. (2015) 61. Joergens et al. (2001) 62. Kraus et al. (2013) 63. Hillenbrand et al. (1992) 64. Kenyon et al. (1990) 65. Brown et al. (2009) 66. van Leeuwen (2007) 67. Riaud et al. (2006) 68. López-Martínez & Gómez de Castro (2015) 69. Moór et al. (2013) 70. Cieza et al. (2010) 71. Rebull et al. (2010) 72. Hughes et al. (1994) 73. Carpenter et al. (2014) 74. Houk (1982) 75. Rich et al. (2015) 76. Prato et al. (2003) 77. Debes et al. (2013) 78. Fernandez et al. (1995) 79. Luhman et al. (2010) 80. Bertout et al. (2007) 81. Wichmann et al. (1996) 82. van Boekel et al. (2005) 83. White & Hillenbrand (2004) 84. Espaillat et al. (2010) 85. Houk (1978) 86. Leinert et al. (1993) 87. Mendigutía et al. (2014) 88. Köhler et al. (2000a) 89. Caballero & Solano (2008) 90. Gregorio-Hetem & Hetem (2002) 91. Metchev et al. (2004) 92. Yudin et al. (1999) 93. Houk & Smith-Moore (1988) 94. Wichmann et al. (1998) 95. Comerón (2008) 96. Kaas et al. (2004) 97. Wilking et al. (2005) 98. Makarov (2007) 99. Neuhäuser et al. (2000)

^a Inferred from its T_{eff} and the spectral type vs. T_{eff} relation of Pecauc & Mamajek (2013)

Using the extinction law of Cardelli et al. (1989), we first corrected the interstellar extinctions, which however only weakly influence most of our YSO targets ($< \sim 0.5$ mag; see Table 5). Adopted parameters of distance and age in Table 5 are used to calculate mass in jovian mass and separation in AU. Figures 12 and 13 show 5σ detection limit of mass with bright and faint YSOs as a function of AU. In this case, our observations could be sensitive to smaller exoplanets around the fainter YSOs than brighter YSOs, because the central stars are fainter. This figure shows that we can set typical upper limit of 5–10 M_J at a few tens of AU. Our results can discuss exoplanets outside 100 AU and brown dwarfs in the solar-system scale. Because Orion Nebula Cluster, Serpens-Aquila and Perseus are located farther than the other star forming regions (see Tables 1, 5), it is unable to constrain planetary-mass companions within 100 AU in these star-forming regions. Some contrast curves are influenced by the bright companions (see Section 4.1), producing the biases in the contrast determinations.

4.3. Results of Individual Companion Survey

4.3.1. TYC 4496-780-1

This isolated T Tauri star in front of the Cepheus complex has strong NIR and FIR excess and $H\alpha$ accretion signature (Guillout et al. 2010).

SEEDS observed this system in 2012 July with qPDI+ADI mode. We detected a bright source at $\sim 1''.5$. Guillout et al. (2010) suggested that this system is a spectroscopic-binary system; we find that our detected object is possibly a stellar component of the pair. Since we have no follow-up observations of this target and this detected source is very bright, we do not consider that this object is a planetary-mass companion candidate.

4.3.2. HD 21997

This A3 star is a member of the Columba moving group (Moór et al. 2006, 2013), which is as old as ~ 30 Myr (Torres et al. 2008). However, its SED shows a transitional-like disk rather than debris disk (Moór et al. 2013). SEEDS therefore observed HD 21997 in the YSO category.

We reduced the data taken in 2013 January with sPDI+ADI and $0''.4$ mask, detecting no companion candidates.

4.3.3. *LkH α 330*

LkH α 330 is a T Tauri star in the Perseus star forming region. This star has an SED of transitional disk, and a gap and asymmetric structure was observed in the disk (e.g. Brown et al. 2008, 2009; Isella et al. 2013).

SEEDS observed LkH α 330 three times in 2011 December using sPDI+ADI with $0''.4$ mask, 2014 October and 2015 January using qPDI+ADI mode without masks. Our data reductions for all data detected no companion candidate. We constrained the potentially existing exoplanet smaller than $60 M_J$ at 50 AU, $16.5 M_J$ at 100 AU.

4.3.4. *IRAS 04028+2948*

This Herbig Ae/Be star in the Taurus star forming region has an SED with the IR excess and concavity at MIR range (Kenyon et al. 1990; Rebull et al. 2011).

We reduced the data observed in 2012 December with qPDI+ADI mode and detected no companion candidates in its FOV. We set a detection limit of $20 M_J$ at 50 AU.

4.3.5. *IRAS 04125+2902*

This T Tauri star is a $4''.0$ binary system in the Taurus star forming region and has a transitional disk (Kim et al. 2013; Espaillat et al. 2015).

We reduced the data taken in 2013 November and in 2014 January with sPDI+ADI mode and confirmed this system to be a binary system. We did not detect any other companion candidates in its FOV.

4.3.6. *LkCa 4*

LkCa 4 is a T Tauri star in the Taurus star association and has an SED indicative of a class III object (Furlan et al. 2006; Howard et al. 2013). The spectroscopic study derived Li abundance of this system (Sestito et al. 2008).

SEEDS observations were carried out in 2012 November with qPDI+ADI, resulting in no detection of companion candidates in its FOV.

4.3.7. *Elias 1*

Elias 1 (= V892 Tau) is a Herbig Ae/Be star in a $\sim 4''$ binary system, which is a member of Taurus association, and that possesses a circumbinary disk (Monnier et al. 2008), which is interesting to study the disk property.

This object was observed in 2013 February with sPDI+ADI+ $0''.4$ mask. We confirmed the stellar companion but did not detect any other companion candidates.

4.3.8. *BP Tau*

This T Tauri star in the Taurus star forming region was observed by resolving the disk, in which CO appears to start to be depleted (Dutrey et al. 2003).

SEEDS observations were carried out in 2012 September with qPDI+ADI mode. We detected a point source at $\sim 3''.1$ near the edge of FOV. In order to discuss proper motion of the companion candidate, we used HST/NICMOS and Subaru/CIAO data. Our CPM test showed that this source is likely a background star. We used the proper motions reported in Zacharias et al. (2012) ($\mu\alpha=7.4\pm 1.2$, $\mu\delta=-28.4\pm 0.7$ [mas/yr]). However, NICMOS data are saturated and CIAO data are masked, which means these data have large astrometric uncertainty. Judging whether this object is a companion or a background star requires follow-up observations. We do not conclude that this object is a background star.

4.3.9. *V819 Tau*

V819 Tau is a class III object in the Taurus association and has an excess at $24 \mu\text{m}$ and FIR (Furlan et al. 2006; Luhman et al. 2009), which may arise from a transitional disk.

HiCIAO images taken in 2012 January with qPDI+ADI detected no companion candidates in its FOV.

4.3.10. *RY Tau*

RY Tau is a T Tauri star in the Taurus star forming region. Isella et al. (2010a) resolved this disk and reported an inner gap, which suggests that a planet with a mass less than $5 M_J$ exists between 10 and 50 AU from the primary star.

HiCIAO images taken in 2011 January with sPDI+ADI+ $0''.4$ mask and in 2014 October with sPDI+ADI detected a faint source at $5''$. We do not include this object as a companion candidate.

4.3.11. *T Tau*

T Tau was first-selected protostar as a new type of variable star (Joy 1945). This YSO is a well-studied triple system in the Taurus-Auriga star forming region. T Tau is now called T Tau N and the companions are called T Tau Sa and T Tau Sb. These components of the system have IR excesses (Hogerheijde et al. 1997; Ratzka et al. 2009).

SEEDS observation carried out in 2015 January had few rotation angle and we could not discuss exoplanets located within $2''.3$.

4.3.12. *IP Tau*

This T Tauri star in the Taurus star forming region has a pre-transitional disk (Espaillat et al. 2011).

SEEDS observation was carried out in 2011 December with qPDI+ADI mode. We reduced the data and detected no companion candidates. Calculation of detection limit excludes possible companions more massive than $14 M_J$ at 50 AU.

4.3.13. *DG Tau*

This T Tauri star is a $\sim 1'$ -separation binary system (e.g., Rodmann et al. 2006) in the Taurus star forming region and has a resolved image of its circumstellar disk (Isella et al. 2010a), accompanied by the radio jet (Lynch et al. 2013).

We did not detect any point sources in the FOV of the qPDI+ADI data taken in 2015 January.

4.3.14. *UX Tau*

UX Tau A is a T Tauri binary in the Taurus star forming region. Espaillat et al. (2007) reported a transitional disk around UX Tau A. SEEDS reported that the polarization degrees largely vary over the disk, indicating a thin disk with dust grains (Tanii et al. 2012).

We reduced the HiCIAO data taken in 2013 November with qPDI+ADI mode and confirmed the stellar companion at a separation of $\sim 2''.7$. We did not detect any other companion candidates. For detection limit, we could not discuss the inner part of 400 AU, which were automatically masked by LOCI.

4.3.15. *HL Tau*

HL Tau is a T Tauri star associated with the Taurus star forming region. Previous studies using Subaru/CIAO (Tamura et al. 2000) has reported an asymmetric (C-shaped) feature and different color pattern on its disk (Murakawa et al. 2008). Recently, multi ring feature in the mid-plane of the disk was reported by ALMA observations (ALMA Partnership et al. 2015), with which Akiyama et al. (2016) discussed planet formation in this system. Testi et al. (2015), using Large Binocular Telescope Interferometer mid-infrared camera (LBTI/LMIRcam), tried to find companions of HL Tau, but resulting in non detection and upper limit on exoplanets of $\sim 10\text{--}15 M_J$ at 70 AU.

SEEDS observations were conducted in 2015 January after ALMA press release. At the observations, the HL Tau's PSFs largely varied, possibly due to bad weather condition. In the final image made through our data reductions, there were residuals of stellar halo, preventing us from detecting any companion candidates.

4.3.16. *L1551-51*

L1551-51 is a T Tauri star in the Taurus association. Its SED classifies the star into class III object (Luhman et al. 2010; Howard et al. 2013). Martin et al. (1994) derived Li abundances of this YSO from spectroscopic observations.

We reduced the data taken in 2012 November with qPDI+ADI and detected no companion candidates.

4.3.17. *GG Tau*

GG Tau is a T-Tauri star associated with the Taurus star forming region. This star is one of a quadruple system (Aa, Ab, Ba, Bb White et al. 1999, ;) and surrounded by the circumstellar disk (e.g., Krist et al. 2005). SEEDS reported the gap and asymmetric features in its disk (Itoh et al. 2014; Yang et al. 2016).

HiCIAO observed GG Tau twice, one of which were taken for short exposure time and LOCI cannot be applied. Thus we use only the same data as those presented by Itoh et al. (2014), which were taken in 2011 September using sPDI+ADI mode and $0''.6$ occulting mask. The occulting mask is large and this observation did not obtain the field rotation large enough to examine the inner region of the planetary system. As a result, the inner part within 300 AU is masked after the LOCI data reduction, detecting no companion candidate.

4.3.18. *L1551-55*

This T Tauri member of the Taurus star forming region is classified into class III (Luhman et al. 2010; Howard et al. 2013). Magazzu et al. (1992) observed this YSO and estimated Li abundance.

SEEDS observation was carried out in 2012 November with qPDI+ADI mode. We did not detect any companion candidates in its FOV.

4.3.19. *DL Tau*

DL Tau is a T Tauri member of the Taurus association and has an infrared excess (Hartmann et al. 2005; Andrews & Williams 2007). Andrews & Williams (2007) resolved the disk around DL Tau.

HiCIAO images observed in 2014 October with qPDI+ADI did not detect any companion candidates.

4.3.20. *DM Tau*

This T Tauri star belongs to Taurus star forming region. Previous studies reported this system has a transitional disk (Calvet et al. 2005; Andrews & Williams 2007). Andrews et al. (2011) reported a gap at ~ 20 AU from the central star.

SEEDS observation was carried out in 2009 December with sPDI+ADI mode. Our data reduction detected no companion candidates.

4.3.21. *CI Tau*

CI Tau is a T Tauri star in the Taurus star forming region and has an infrared excess in its SED and its disk was resolved (Andrews & Williams 2007).

This system was observed in 2012 September with qPDI+ADI mode. We did not detect any companion candidates in its FOV.

4.3.22. *DN Tau*

DN Tau, a T Tauri member of the Taurus association, has an IR excess from MIR to FIR in its SED (Najita et al. 2007; Andrews & Williams 2007) and its disk was resolved by sub-mm observations (Andrews & Williams 2007).

We reduce HiCIAO data taken in 2009 December with sPDI+ADI, resulting in no detection of point sources.

4.3.23. *LkCa 14*

LkCa 14 is a T Tauri star in the Taurus association. This system is classified as class III object and has an IR excess (Hartmann et al. 2005; Dent et al. 2013), which may imply a transitional disk.

HiCIAO images taken in 2011 December with sPDI+ADI detected no companion candidates in the FOV.

4.3.24. *LkCa 15*

LkCa 15 is a T Tauri star in the constellation of Taurus and has a transitional disk (Najita et al. 2007; Espaillat et al. 2007), which has a gap structure revealed by various-wavelength imaging observations (e.g., Piétu et al. 2006; Thalmann et al. 2010, 2014, 2015). Furthermore, the companion candidates have been reported and investigated by Keck/NIRC2 observation (Kraus & Ireland 2012). The Large Binocular Telescope (LBT) confirmed the companion candidates and MagAO

observation discovered the $H\alpha$ emission that implies mass accretion (Sallum et al. 2015).

Thalmann et al. (2010) used the SEEDS data taken in 2009 December with sPDI+ADI mode. In addition to this observation, LkCa 15 was observed in 2010 January with ADI, in 2010 December with sPDI+ADI, in 2011 January with sPDI+ADI, and in 2013 November with qPDI+ADI mode. We analyzed all of these data and detected no point sources. The inner exoplanets detected by Sallum et al. (2015) are located in the strong self-subtraction region and LOCI automatically masked. In the first and fourth epoch, however, we recognized a similar pattern of signal in the final maps as Gemini/NIRI images (Thalmann et al. 2014), though these patterns are low S/N ratio of ~ 2 –4. We think that these signals are protoplanetary disks but do not discuss the disk feature. We finally estimated upper limit of 5 M_J at 30 AU, 4.5 M_J at 50 AU, 3.5 M_J at 70 AU.

4.3.25. *LkH α 332 G1*

This T Tauri star is a $\sim 0''.23$ binary system in the Taurus association (Leinert et al. 1993). Previous studies reported accretion signatures (e.g. McCabe et al. 2006). The SED has a IR excess which may represent a transitional disk (Hartmann et al. 2005).

We observed this system in 2013 January with sPDI+ADI and $0''.4$ mask. The occulting mask prevented us from confirming the stellar companion. HiCIAO image detected a bright point source at the edge ($\sim 10''$) of FOV and we think this object is a stellar companion or background star due to its wide separation.

4.3.26. *GO Tau*

This T Tauri star is a member of the Taurus star forming region. Its SED is appeared to be that of a transition disk (Najita et al. 2007). The disk was imaged at submillimeter wavelengths (Andrews & Williams 2007).

SEEDS observed GO Tau in 2009 December with sPDI+ADI mode. We detect a point source at $4''.9$, but did not re-observe this system. We exclude this object from exoplanet candidate because its separation is too large. We did not detect any other companion candidates.

4.3.27. *GM Aur*

GM Aur is a T-Tauri star of the Taurus association. HST/NICMOS resolved the protoplanetary disk (Schneider et al. 2003). The SED of GM Aur represents a transitional disk (Calvet et al. 2005; Najita et al. 2007; Espaillat et al. 2010), whose cavity was detected by submm observations (e.g. Hughes et al. 2009; Andrews et al. 2011). Spectroscopy from FUV to NIR range has been executed (Ingleby et al. 2015) and theoretical simulation suggests a gap in the disk (e.g. Espaillat et al. 2010).

This object was observed in 2010 December with qPDI+ADI mode and 2011 December with sPDI+ADI mode. We reduced these data but detect no signal. We calculated contrast of both data and show the better-contrast data on Table 4. Finally, we estimated upper limit as 2.5 M_J at 50 AU and 1.5 M_J at 100 AU.

4.3.28. *LkCa 19*

This class III YSO is a T Tauri star in the Taurus star forming region (Hartmann et al. 2005; Howard et al.

2013). This system has an IR excess at $\lambda = 24\mu\text{m}$ and can be thought to have a transitional disk (Hartmann et al. 2005; Luhman et al. 2010).

We reduced the data observed in 2011 December with sPDI+ADI and detected a point source at $\sim 4''.4$ separation. We do not include this object among companion candidates due to its very wide separation.

4.3.29. *AB Aur*

AB Aur is a Herbig Ae/Be star in the Taurus association. This relatively-bright star has a protoplanetary disk resolved by various instruments (e.g., Oppenheimer et al. 2008; Perrin et al. 2009). The CIAO and HiCIAO observations revealed an asymmetric feature at ~ 50 –500 AU (Fukagawa et al. 2004; Hashimoto et al. 2011).

We reduced the data taken in 2009 December with sPDI+ADI mode that is different from Hashimoto et al. (2011), who reported HiCIAO data taken in 2009 October with only PDI mode. We did not detect any point sources. We then calculated upper limit of the mass of potentially existing exoplanets to be 13 M_J at 100 AU.

4.3.30. *SU Aur*

SU Aur is a T Tauri star associated with the Taurus association. This system had been reported to have an IR excess (e.g. Hartmann et al. 2005) and a nebulosity (Nakajima & Golimowski 1995). SEEDS revealed the asymmetric and tail structures in this system (de Leon et al. 2015).

SU Aur was observed in 2014 January and in 2014 October with qPDI+ADI mode. We reduced these data and did not detect any companion candidate. Detection limit is estimated to be 10 M_J at 50 AU.

4.3.31. *V397 Aur*

This class III YSO in the Taurus star forming region has an IR excess (Hartmann et al. 2005; Furlan et al. 2006), which is indicative of a transitional disk.

SEEDS observation was carried out in 2011 December with sPDI+ADI mode and detected a point source at $\sim 6''$. We do not include it in companion candidates because of very wide separation.

4.3.32. *RX J0458.7+2046*

RX J0458.7+2046 (V1207 Tau) is a T Tauri star in the Taurus star forming region. Wichmann et al. (2000) estimated Li abundance of this system and Wahhaj et al. (2010) reported this system has a diskless SED.

HiCIAO observation was conducted in 2012 November with qPDI+ADI mode and in 2015 December with sPDI+ADI. We detected a point-like source at the edge of FOV. The follow-up observation in 2015 showed the source was false positive and we did not detect any companion candidates within 400 AU.

4.3.33. *MWC 480*

MWC 480 is a relatively-bright, Herbig Ae/Be star in the Taurus association and has a full disk so far imaged at multiple wavelengths (Piétu et al. 2006; Kusakabe et al. 2012; Grady et al. 2010), with the observations of CO emissions from the disk (Akiyama et al. 2013).

We reduced the data observed in 2010 January with sPDI+ADI mode and detected 2 sources at $\sim 4''$ and 2 sources at $\sim 6''$, which are not included in planetary-mass companion candidates due to their large separations.

4.3.34. *HD 34282*

HD 34282 is a Herbig Ae/Be star associated with the Orion Nebula Cluster. It has a large disk (Merín et al. 2004) with the CO emissions (Dent et al. 2005), whose image was previously resolved (Piétu et al. 2003). A recent study, published after our SEEDS observations for HD 34282, suggested that the disk is a transition disk (Khalafinejad et al. 2016).

SEEDS observation was carried out in 2011 December with sPDI+ADI and $0''.4$ mask. We detected no companions within its FOV.

4.3.35. *MWC 758*

MWC 758 is a Herbig Ae/Be star in the Taurus star forming region. This system has been known to have a transitional disk (Isella et al. 2010b) and CO emission in its disk (Dent et al. 2005). Grady et al. (2013) and Benisty et al. (2015) reported the obvious asymmetric features and spiral arms, which can be caused by giant planets. Dong et al. (2015) discussed the potential exoplanets that can make the asymmetric and arm features.

SEEDS observed MWC 758 in 2011 December with sPDI+ADI plus $0''.4$ mask and qPDI+ADI, and 2013 October with qPDI+ADI mode. We analyzed these data and detected a point source at $\sim 2''.5$, which was concluded as a background star by Grady et al. (2013). We did not detect any other companion candidates and finally exclude the possibility that there is an exoplanet with a mass larger than $16 M_J$ outside 150 AU.

4.3.36. *CQ Tau*

This Herbig Ae star in the Taurus association has a disk in which CO emission was reported (Dent et al. 2005). By investigating carbon chemistry of the disk, Chapillon et al. (2010) suggested that CQ Tau's disk is likely a transitional disk. Previous studies discussed radial profile of the disk (e.g. Doucet et al. 2006; Trotta et al. 2013).

SEEDS observation carried out in 2012 January with qPDI+ADI, in 2014 October with sPDI+ADI+ $0''.3$ mask and 2015 December with sPDI+ADI. We detected a point source at $\sim 2''.2$ and our CPM test revealed that this object is likely a background star. We adopted the proper motions reported in Zacharias et al. (2012) ($\mu\alpha = 2.2 \pm 0.6$, $\mu\delta = -25.5 \pm 0.7$ [mas/yr]).

4.3.37. *V1247 Ori*

Previous spectral classifications of V1247 Ori range from F2 to A0 (e.g. Vieira et al. 2003; Kraus et al. 2013). V1247 Ori is a member of the Orion star forming region and shows a dip around $\sim 15 \mu\text{m}$ in the SED, suggesting the presence of a transitional disk (Caballero 2010; Kraus et al. 2013). Kraus et al. (2013) discovered an asymmetric feature in the disk using the Very Large Telescope Interferometer, the Keck Interferometer, Keck-II, Gemini South, and IRTF.

SEEDS observations were conducted three times in 2013 November with sPDI+ADI plus $0''.3$ occulting mask,

in 2014 January with qPDI+ADI and 2015 January with ADI mode. We reduced these data and did not detect any companion candidate. Since this object is located at 385 pc, thus our constraints cannot discuss exoplanets within 100 AU; our observations can constrain the mass of potentially existing objects of $33 M_J$ at 100 AU and $12 M_J$ at 200 AU.

4.3.38. *TW Hya*

TW Hya is the nearest system from the Earth among our whole targets. This T Tauri star is in the TW Hydrae moving group (e.g. Webb et al. 1999; Zuckerman et al. 2001; Brandt et al. 2014b), which is located about 50 pc and is about 10 Myr years old. The declination is very low ($\delta < -30^\circ$), making it relatively difficult to observe this moving group in high airmass. TW Hya has a transitional disk with active accretion reported by its SED (e.g. Calvet et al. 2002; Goto et al. 2012; Menu et al. 2014) and its disk has been resolved in various wavelengths (Krist et al. 2000; Weinberger et al. 2002; Qi et al. 2004). Detailed information of selection criteria is described in Akiyama et al. (2015). SEEDS also observed this system and revealed multi-gap feature at 20 and 80 AU (Akiyama et al. 2015).

We analyzed the same data as reported in Akiyama et al. (2015), which were taken in 2011 March and 2013 January with qPDI+ADI mode. We did not detect any signal and set constraints on detectable mass of exoplanet as 16 and $3 M_J$ at the inner and outer gaps. Akiyama et al. (2015) analyzed the HiCIAO polarized intensity (PI) images and estimated a mass of potential planet, which creates a gap structure, to be lower than $0.7 M_J$ according to the theoretical calculations of Jang-Condell & Turner (2012). Our results are consistent with the predictions of Jang-Condell & Turner (2012) but cannot set stronger constraints.

4.3.39. *PDS 70*

PDS 70 is a T Tauri star in the Centaurus group. The SED of this system implies a transitional disk (Metchev et al. 2004; Riaud et al. 2006) and Riaud et al. (2006) resolved a scattered light disk around PDS 70 (detailed information is described in Hashimoto et al. (2012)).

SEEDS observed this object in 2012 February with qPDI+ADI mode and detected a gap feature (Hashimoto et al. 2012). This gap is so wide as ~ 70 AU that Hashimoto et al. (2012) discuss the possibility of multi planets system. We reduced the same data as mentioned above, detecting a point source at $\sim 2''.2$. Hashimoto et al. (2012) concluded this source is a background star by combining their results of observations and those in Riaud et al. (2006). Thus we did not detect any companion candidate. We estimated the detection limit of $16 M_J$ at 70 AU.

4.3.40. *SAO 206462*

SAO 206462 is a T Tauri star, sometimes called as Herbig F star, and a $\sim 20''$ visual binary system (HD 135354; Augereau et al. 2001). The secondary star is outside the FOV of SEEDS observation. This object is in the constellation of Lupus. SAO 206462 has been predicted to

have a gap from its SED feature (Brown et al. 2007), which was later confirmed by sub-millimeter imaging (Brown et al. 2009).

Muto et al. (2012) revealed spiral arms and asymmetric feature using the SEEDS data, and also discussed potential planets by examining the disk’s geometry. The Submillimeter Array (SMA) and ALMA observations also revealed the inner gap (Brown et al. 2009; van der Marel et al. 2016). Dong et al. (2015) discussed the potential exoplanets that can make the asymmetric features around SAO 206462, as well as MWC 758.

SEEDS observed this system in 2011 May with sPDI+ADI and $0''.4$ occulting mask. After the LOCI data reduction, we detected two point sources. Our identified sources are exterior to 400 AU from SAO 206462. Furthermore, our observations are unable to detect a companion candidate in the gap of disk, due to strong self-subtraction of LOCI-ADI reductions. Finally we set upper limit. Muto et al. (2012) predicted the positions of two potential exoplanets, one of which however is in the software mask of LOCI and cannot be detected even if this planet exactly exists. At $0''.9$, ~ 130 AU where another potential planet could be located, HiCIAO detection limit excludes the probability of planets larger than $3 M_J$. This constraint agrees to the theoretical prediction of mass of the planet (Muto et al. 2012).

4.3.41. HD 139614

This star is a Herbig Ae/Be star associated with the Lupus-Ophiuchus complex, with the dust emissions in the SED (Meeus et al. 1998; Matter et al. 2014) that can be interpreted as a pre-transitional disk (Matter et al. 2014).

We reduced the data acquired in 2014 January with sPDI+ADI and $0''.4$ mask and detected 2 point sources at $\sim 3''.5$ separations. We also detected relatively low SN (~ 4 – 4.5) objects within $1''$ and need follow-up observation. Therefore we did not detect convincing companion candidates within 400 AU.

4.3.42. GQ Lup

GQ Lup is a T-Tauri star in the Lupus star forming region and has the infrared excess with MIR concavity (Dai et al. 2010). In this system, a companion (GQ Lup b) has been discovered by direct imaging (Neuhäuser et al. 2005). The mass estimate of GQ Lup b ranges from 1 to $60 M_J$ (e.g. Neuhäuser et al. 2005; Seifahrt et al. 2007; Lavigne et al. 2009).

SEEDS observed this planetary system in 2013 May with both qPDI+ADI mode and sPDI+ADI mode plus $0''.4$ occulting mask. We confirmed the companion (see Figure 3 and Table 6). Our qPDI+ADI data reductions derived the separation and position angles of GQ Lup b to be $(\rho, \theta) = (0''.723 \pm 0''.012, 277^\circ.38 \pm 1^\circ.40)$. Our results did not deviate from the measurements in Neuhäuser et al. (2008) but had larger errors of position angle because the seeing was bad and central star of science frames are masked or strongly saturated. Neuhäuser et al. (2008) found that the separation between the companion and central star decreases by ~ 2 – 3 mas/yr due to its orbital motion (Figure 2 (a) of Neuhäuser et al. 2008). The extrapolation of the separation decrease calculated by Neuhäuser et al. (2008) is

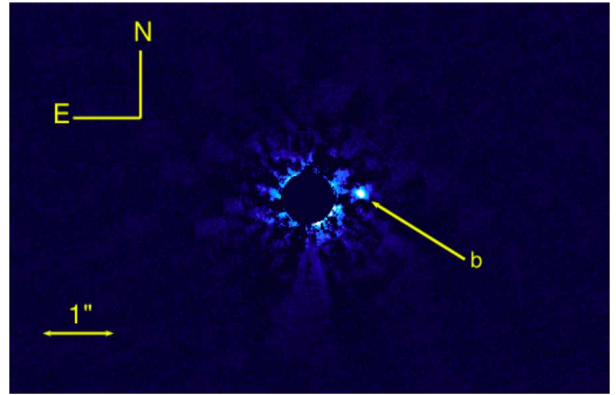


Figure 3. Subaru/HiCIAO H -band image of GQ Lup b taken in 2013 May. The central star is masked. North is up and east is left.

consistent with our data, which can help to constrain the companion’s orbital motion.

Our photometric estimation resulted in deriving a mass of GQ Lup b to be ~ 15 – $20 M_J$. We also detected one more point source at $6''$ but this object has been concluded as a background star (e.g. Neuhäuser et al. 2008). We also excluded the possibility of exoplanets more massive than $16 M_J$ at 70 AU.

4.3.43. HIP 77545

This Herbig Ae/Be star is a member of Upper Sco. Carpenter et al. (2009) detected an infrared excess at $24 \mu\text{m}$ but did not detect the excesses at 8 and $16 \mu\text{m}$.

SEEDS observations were in 2012 May with sPDI+ADI and 2014 January with ADI. We detected a point source at $3''.8$ and two additional sources at the wider separations in the second data. On the other hand, the first data detected no point sources with the significant SN ratios and need more follow-up observations. Given that this system is located about 120 pc, we do not include these sources among companion candidates.

4.3.44. HIP 77911

HIP 77911 is a Herbig Ae/Be star in the Upper Sco association. Previous study has reported a debris disk (Carpenter et al. 2009; Mathews et al. 2013).

This system was observed in 2012 May with sPDI+ADI and 2014 January with ADI mode. We reduced the data and detect some point sources at separations larger than $4''$ (~ 600 AU). We do not count them as companion candidates.

4.3.45. IM Lup

IM Lup is a T Tauri star in the Lupus association. The IM Lup’s protoplanetary disk has been imaged from optical to radio wavelengths (Pinte et al. 2008; Panić et al. 2009). The surface density of the disk greatly changes at ~ 400 AU (Panić et al. 2009).

IM Lup was observed in 2014 June with qPDI+ADI mode. After the data reduction, we detected two companions at $2''$ and $2''.5$. Mawet et al. (2012) has reported the point source closer to the central star as a background star by calculating its proper motion with the VLT/NACO and HST/NICMOS data, but the more distant one has not been reported, requiring more follow-up observations for the clarification of this object.

4.3.46. HD 142527

HD 142527 is a relatively-bright, Herbig Ae/Be star in the constellation of the Lupus association. Some studies have reported the gap and asymmetric structure of the disk in this system (e.g. Fukagawa et al. 2006; Verhoeff et al. 2011; Fukagawa et al. 2013; Avenhaus et al. 2014). The possibility of companion existences was examined by (Biller et al. 2012).

SEEDS observed HD 142527 in 2011 May with sPDI+ADI combined with $0''.4$ mask and in 2012 April with sPDI+ADI mode. We detected 2 high-SNR point sources and one marginally-detected source in each data set, which are located at distances larger than 550 AU. Therefore we exclude them from the list of companion candidates. Furthermore, we estimated the upper limit of detectable companion mass of $20 M_J$ at 50 AU.

4.3.47. RX J1603.9-2031A

This T Tauri star is one of a $\sim 4''$ binary system in the Upper Sco association (Köhler et al. 2000b) and shows an infrared excess (Carpenter et al. 2009; Mathews et al. 2013).

SEEDS images taken in 2012 July with qPDI+ADI detected no companion candidates and set upper limit of potential exoplanet to be $5 M_J$ at 50 AU from the central star.

4.3.48. RX J1604.3-2130A

RX J1604.3-2130A (USco J1604) is a T Tauri star of the Upper Sco association and has an SED indicative of transition disk (Dahm & Carpenter 2009). This transition disk shows a gap feature revealed by SMA and Subaru (SEEDS) (Mathews et al. 2012; Mayama et al. 2012). Mayama et al. (2012) reported the presence of an arc-like structure, inside RX J1604's ring, at the west side of the star. This structure is now suspected to be an artifact.

We reduced HiCIAO data observed in 2012 April with qPDI+ADI mode, which have been used by Mayama et al. (2012). We did not detect any companion candidate and set detection limit of the mass of potentially existing exoplanet as $5.5 M_J$ at 50 AU.

4.3.49. SZ 91

This T Tauri star is a member of the Lupus molecular cloud (Hughes et al. 1994) with a transitional disk (e.g. Merín et al. 2008; Romero et al. 2012). Tsukagoshi et al. (2014) also used the HiCIAO data and spatially resolve the inner ($r \sim 65$ AU) and outer ($r \sim 170$ AU) disks.

We used the same data as reported by Tsukagoshi et al. (2014), which were taken in 2012 May with sPDI+ADI mode. As a result, we detected two point sources at $\sim 4''.2$ and $\sim 9''$. We do not count them in companion candidates and set upper limit of $6.5 M_J$ at 70 AU.

4.3.50. HIP 78996

This Herbig Ae/Be star associated with the Upper Sco association has a debris disk (Carpenter et al. 2009; Mathews et al. 2013).

SEEDS observations were carried out in 2011 May with sPDI+ADI+ $0''.4$ mask and in 2013 May with sPDI+ADI.

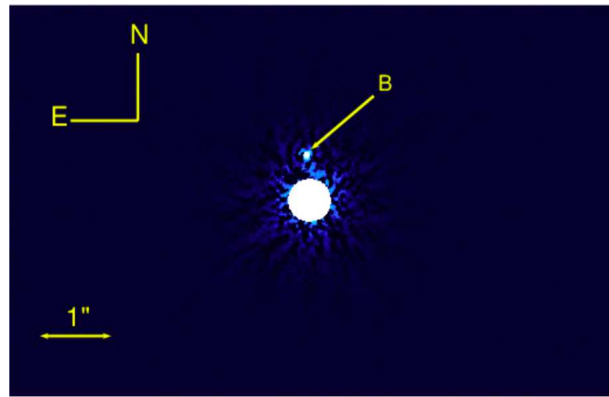


Figure 4. Subaru/HiCIAO H -band image of a companion around HIP 79462 taken in 2014 April. The central star is masked. North is up and east is left.

We detected a point source at $3''.5$ from the primary star. Our CPM test indicates that this object is likely a background star. For the proper motion test, we used the proper motions reported in Zacharias et al. (2012) ($\mu\alpha = -11.8 \pm 0.9$, $\mu\delta = -23.2 \pm 0.9$ [mas/yr]).

4.3.51. V1094 Sco

This T Tauri star in the Lupus association has a full disk (Tsukagoshi et al. 2011; Bustamante et al. 2015).

We reduced the data taken in 2011 May with sPDI+ADI+ $0''.4$ mask and detected 5 point sources at $5''.5$ – $9''$ (~ 850 – 1400 AU). The outer radius of the disk was estimated to be 320 AU (Tsukagoshi et al. 2011); we therefore do not discuss possibility of companion for these sources.

4.3.52. HIP 79462

HIP 79462 is a T Tauri star in the Upper Sco association. This system has a debris disk (Carpenter et al. 2009; Dahm et al. 2012).

SEEDS observed HIP 79462 three times with only ADI mode in 2012 April, 2014 April and 2015 April. We detected a companion, HIP 79462B (see Figure 4 and Table 6) at $(\rho, \theta) = (0''.648 \pm 0''.013, 3^\circ 35' \pm 1''.07)$; these values are derived from 2012 April data. The H -band contrast is 4.2 ± 0.3 magnitudes; this gives an absolute H -band magnitude of 5.9 ± 0.3 assuming a distance of 142 pc and an H -band magnitude of 7.43 ± 0.07 for the primary (Cutri et al. 2003; Skrutskie et al. 2006). We have no measurements of the companion's color. The COND03 and Solar-metallicity BT-Settl models at an age of 10 Myr (Baraffe et al. 2003; Allard et al. 2011) give an effective temperature of ~ 3200 K and a mass of $0.2 M_\odot$, well above the minimum mass for hydrogen ignition. Pecaut & Mamajek (2013) list a spectral type of M4 at $T_{\text{eff}} = 3200$ K.

4.3.53. HIP 80088

HIP 80088 is a Herbig Ae/Be star in the Upper Sco association. Its SED indicates the presence of a debris disk (Carpenter et al. 2009; Mathews et al. 2013).

This object was observed in 2012 July twice, using ADI-only and sPDI+ADI mode. We detected 2 point sources at $\sim 8''$ and $10''$ but do not include them among companion candidates due to their wide separations.

4.3.54. *IRAS 16225-2607*

This T Tauri star is a member of the Ophiuchus star forming region. The previous study reported an SED that appears to be a transitional disk’s SED (Furlan et al. 2009). Furlan et al. (2009) did not report a stellar companion in this system, but Elliott et al. (2015) and Ansdell et al. (2016) reported a stellar companion at $\sim 0''.9$.

SEEDS observation was in 2012 November with qPDI+ADI mode. We detected the same source at $\sim 1''.0$ separation as Elliott et al. (2015) reported. Photometric result showed this object is more massive than brown dwarf ($\Delta H \sim 1$ mag). Another point source was detected, which is located at $1''.5$ from the central star and near the bright stellar companion, and was therefore possibly affected by the companion, needing the follow-up observations.

4.3.55. *DoAr 25*

DoAr 25 is a T-Tauri star in the constellation of Ophiuchus and its SED indicates less evolved version of transitional disk (Andrews et al. 2008).

We reduced the 2 data taken in 2012 May with qPDI+ADI mode and 2014 January with ADI mode. We do not detect any signal in the first data, but detected a companion candidate in the second data. This object is separated by $4''.5$ from the central star, and we thus assume that this is not a substellar companion. Our calculated contrast exclude the possibility of exoplanets more massive than $13 M_J$ at 70 AU.

4.3.56. *HD 148040*

This T Tauri star is a member of the Upper Sco association. This system has a $24 \mu\text{m}$ excess but lack a $70 \mu\text{m}$ excess (Chen et al. 2005, 2011).

HiCIAO images were taken in 2012 May with sPDI+ADI and in 2015 April with ADI mode. We detected a point source at $\sim 3''.9$ but the CPM test revealed this object to be a background star. We used the proper motions reported in Zacharias et al. (2012) ($\mu\alpha = -11.4 \pm 1.4$, $\mu\delta = -22.0 \pm 1.0$ [mas/yr]).

4.3.57. *DoAr 28*

DoAr 28 is a T Tauri star associated to the ρ Ophiuchus association. This system has a transitional disk with an asymmetric and hook feature (McClure et al. 2010; Rich et al. 2015). A companion candidate discovered at $\sim 1''$ was concluded to be a background star using the SEEDS data (Rich et al. 2015).

We reduced the same data as Rich et al. (2015) taken in 2012 May and 2014 January with qPDI+ADI mode. We detected the companion candidate and conducted the CPM test, confirming this object to be a background star.

4.3.58. *SR 21*

SR 21 is a T Tauri star of the Ophiuchus star forming region and is classified as one of a $\sim 6''.4$ binary system (Prato et al. 2003). This disk has a transitional disk feature and a cavity identified by the SED data and sub-mm observations (Furlan et al. 2009; Andrews et al. 2009; Brown et al. 2009; Pérez et al. 2014; van der Marel et al.

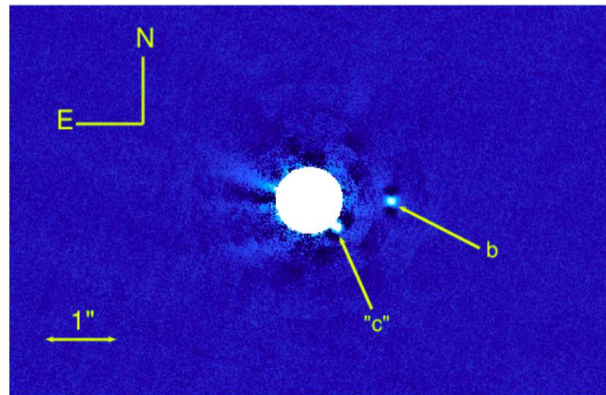


Figure 5. Subaru/HiCIAO Y-band image of a companion around ROXs 42B taken in 2014 June. The central star is masked. North is up and east is left.

2016). Nevertheless, Follette et al. (2013) reported no cavity in the NIR scattered-light image.

For SEEDS observation, SR 21 was observed in 2011 May with qPDI+ADI mode. We reduced this data set and detected a feature like a point source, which has a SN ratio of 4.5. However, there are the remnants of spiders in the final image and this source is detected near these remnants. Therefore we assume this signal is likely effected by the spiders. We also ruled out possibility of existing exoplanet smaller than $11 M_J$ at 70 AU.

4.3.59. *Oph IRS 48*

Oph IRS 48 is a Herbig Ae/Be star associated with the Ophiuchus association. The disk of its system shows a gap feature (Brown et al. 2012), which possibly originates from a companion (van der Marel et al. 2013, 2014).

We reduced the SEEDS data taken in 2013 May with qPDI+ADI mode and did not detect any signal. We then set upper limit of $30 M_J$ at 50 AU.

4.3.60. *ROXs 42B*

ROXs 42B is a T Tauri star in the ρ Ophiuchus star forming region. This system has a companion ROXs 42B b and a companion candidate “c” (Currie et al. 2014b). We follow the expression of “c” in Currie et al. (2014b) because Kraus et al. (2014) and Currie et al. (2014a) independently argued that this object is likely a background star.

SEEDS observed ROXs 42B in 2014 June with ADI mode. We reduced the data and confirmed the companion b and “c” (see Figure 5 and Table 6). They are located at $(\rho, \theta) = (1''.14 \pm 0''.004, 269.7 \pm 0.17)$ and $(0''.55 \pm 0''.006, 228.7 \pm 0.64)$, respectively. Our results will help discuss the orbital motion of the companion. However, there were no reference frames in this observation and these errors may be underestimated. This follow-up observation after Currie et al. (2014b,a) was conducted in Y-band ($\sim 0.97\text{--}1.07 \mu\text{m}$), which is different from typical HiCIAO imaging band. Therefore we use this data as confirmation of the companion and do not discuss the detection limit.

4.3.61. *ROX 44*

ROX 44 is a T Tauri star associated with the Ophiuchus star forming region. This system has a (pre-)transitional disk (Andrews et al. 2009; Espaillat et al. 2010).

We analyzed SEEDS data taken in 2011 May with qPDI+ADI and 2012 May with sPDI+ADI mode. We detected a point source at $\sim 2''.3$ in the first-epoch data. In the second-epoch data, this companion candidate is located at the inner region where self-subtraction is significant. We conducted the classical ADI data reduction (Marois et al. 2006) with the second data to avoid self-subtraction, but did not detect the candidate. We also have a trouble in making the fits header at the first-epoch data, in which the angular offset was mistakenly recorded. Thus we had to assume the offset from the other parameters in the header. We used HST/WFC3 data taken in 2014 October to check proper motion. We subtracted the 180° rotated image from the original image and confirmed a point source at a similar position. The PSF of central star is heavily saturated, making the centroid measurements uncertain. Because of the large uncertainties and the trouble in our fits header, we still include this object among companion candidates and we need the more follow-up observations. We finally set lower limit of detectable mass of potential companions to be $3 M_J$ at 70 AU.

4.3.62. *RX J1633.9-2442*

This T Tauri star is a member of the Ophiuchus molecular cloud and has a transitional disk (Cieza et al. 2010, 2012; Orellana et al. 2012).

SEEDS observed this object in 2014 April with qPDI+ADI mode and detected no companion candidates in its FOV. We then estimated detection limit to be $9 M_J$ at 50 AU.

4.3.63. *HD 169142*

HD 169142 is a Herbig Ae/Be type, relatively bright star isolated from star forming regions (Dent et al. 2006). Thus, we adopt the stellar parameters individually estimated for HD 161492 itself (see Table 5). The HD 169142's disk has a gap (Grady et al. 2007; Quanz et al. 2013b) and an asymmetric feature (Quanz et al. 2013b), and a companion candidate (Reggiani et al. 2014).

SEEDS observations were conducted in 2011 May and 2013 May with sPDI+ADI plus a $0''.4$ mask. The PDI data reduction detected a gap and an asymmetric feature in its disk (Momose et al. 2015). On the other hand, SEEDS images cannot discuss the reported companion candidate which is located within the occulting mask. Other than this companion candidate, we detected a lot of companion candidates (see Figure 6). HD 169142 is located within the Sagittarius constellation and there are a lot of background stars. We then select signals within 400 AU from all detected sources, which resulted in 6 companion candidates in 2011 May. However, only 4 candidates of these objects were detected in the follow-up observation in 2013 May. Then we executed CPM test for the 4 companion candidates; their separations and position angles are listed in Table 7. Figure 7 shows the results of the CPM test. The first observation did not take position reference frame and we may underestimate errors. We consider them to be background stars because they move so fast and similarly. The difference can be

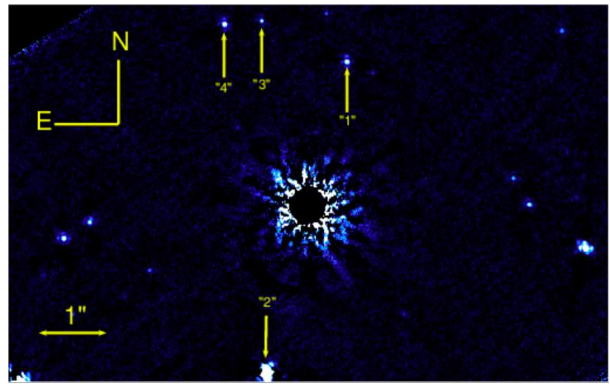


Figure 6. Subaru/HiCIAO *H*-band image of companion candidates around HD 169142 taken in 2011 May. The central star is masked. North is up and east is left. Sources which are not pointed by arrows are outside 400 AU or have low SN. The common proper motions of the No. 1, 2, 3, and 4 sources are tested (see Figure. 7).

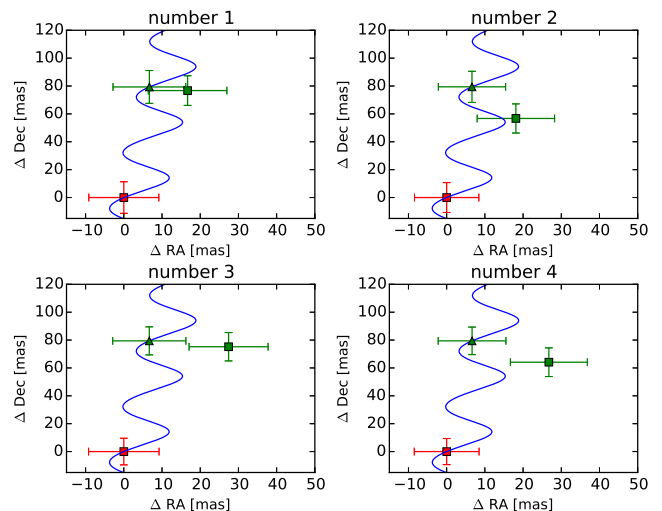


Figure 7. The vertical and horizontal axes are the $\Delta\alpha$ and $\Delta\delta$ of the companion candidates relative to their first-epoch positions. The number represents the object 1, 2, 3, and 4 labeled in Figure 6, respectively. The red square plots correspond to the observed positions at the first epoch (2011 May 23), while the green square plots correspond to the positions observed at the second epoch (2013 May 19). If the companion candidates are background stars, their $\Delta\alpha$ and $\Delta\delta$ changes along with the blue curves, on which the green triangle plots indicate the predicted positions of background stars at the second epoch.

explained by their proper motion and parallax. We assumed proper motion of $(\mu_\alpha, \mu_\delta) = (-3.5 \pm 1.6, -39.9 \pm 1.3)$ [mas/yr] (Zacharias et al. 2012). The two objects remaining without the proper motion tests will be investigated with the next follow-up observations. For detection limit, we constrained the mass of potential companions to $16.5 M_J$ at 50 AU.

4.3.64. *MWC 297*

This Herbig Ae/Be star belonging to the Serpens-Aquila star forming region has a (pre-)transitional disk (Malbet et al. 2007; Rumble et al. 2015). We adopted the distance and age of this YSO from the typical value of the star forming region (see Table 5; Kaas et al. 2004).

HiCIAO images taken in 2012 July with sPDI+ADI mode detected 2 companion candidates at the separations of $\sim 3''$ and $\sim 3''.4$ (>750 AU). We do not include

them in exoplanet candidates due to their large separations. We achieved contrast of 10^{-5} at $1''$ but we were not able to attain the detection limits good enough to detect a planetary-mass companion within 400 AU due to the bright central star.

4.3.65. *RX J1842.9-3532*

RX J1842.9-3532 is a T Tauri star associated with the CrA molecular cloud complex and has a transitional disk (Hughes et al. 2010).

We used the HiCIAO data observed in 2012 September with qPDI+ADI and detected no companion candidates in its FOV. We then constrain the mass of possible exoplanets to $11.5 M_J$ at 50 AU.

4.3.66. *RX J1852.3-3700*

RX J1852.3-3700 is a T Tauri star in CrA and has a transitional disk (Hughes et al. 2010).

SEEDS observation was conducted in 2011 September with sPDI+ADI mode. We detected 6 companion candidates; only one of them is within $3''$ (~ 400 AU) and we exclude the other 5 point sources from companion candidates. This companion candidate also needs follow-up observation to confirm if it is a companion or background object. For detection limit, we set the mass limit of substellar companions to be $6.5 M_J$ at 50 AU.

4.3.67. *HD 179218*

HD 179218 is an isolated Herbig Ae/Be star and located at 240 pc from the Sun. The SED has an IR excess that seems to have a disk with an inner polar cavity (Elia et al. 2004; van der Plas et al. 2008). Liu et al. (2007) resolved its disk and suggested an inner hole of the disk.

The HiCIAO data of this object were taken in 2012 September with sPDI+ADI and $0''.4$ mask in SEEDS.

Our data reduction revealed more than 10 point sources at the radial distances larger than 550 AU. We assume these point sources as background stars or stellar companions. Inner part of $2''.3$ (~ 550 AU) is masked due to the insufficient rotation angle, and thus we cannot derive the detection limit within 400 AU.

4.3.68. *HIP 103763*

HIP 103763 is a triple system in the Cepheus complex. The primary and secondary stars constitute the spectroscopic binary and the separation between each component is 15 mas (e.g. Millan-Gabet et al. 2001; Okamoto et al. 2009). In addition, the third component is separated by $\sim 6''$ from the primary (Li et al. 1994). The primary star has a flare disk that extends to ~ 1000 AU (Okamoto et al. 2009).

HiCIAO observation was conducted in 2011 September with sPDI+ADI+ $0''.4$ mask. We confirmed the bright star at $\sim 3''$, which can be a background object or the third companion.

5. RESULTS AND DISCUSSION OF TOTAL DATA

5.1. *Companion Candidates*

Tables 6 and 7 list all identified point sources within ~ 400 AU. Other companion candidates are described in Section 4.3. GQ Lup, ROXs 42B, HD 169142 and LkCa 15 have been reported to have the candidates of substellar companion including brown dwarf. The observational conditions are explained in Section 4.3. We detected only GQ Lup b and ROXs 42B b (see Table 6), and because objects around HD 169142 and LkCa 15 are located in the inner region where LOCI automatically covers the mask. Furthermore, we did not detect any companion candidates around YSOs whose disks have intriguing features suggesting planet formation such as SAO 206462, MWC 758, and HD 142527.

Table 6
Detected Companions in This Study

HD name	Other name	ΔH (mag)	Separation	Position Angle	Date (HST) and Method
...	GQ Lup	6.7 ± 0.3	$0''.723 \pm 0''.012$ $0''.723 \pm 0''.034$	$277^\circ 38 \pm 1^\circ 40$ $275^\circ 66 \pm 1^\circ 53$	2013 May 17, qPDI+ADI 2013 May 19, sPDI+ADI
145655	HIP 79462	4.2 ± 0.3	$0''.648 \pm 0.013$ $0''.676 \pm 0''.010$ $0''.666 \pm 0''.011$	$3^\circ 35 \pm 1^\circ 07$ $4^\circ 26 \pm 0^\circ 86$ $4^\circ 87 \pm 0^\circ 78$	2012 Apr 11, ADI 2014 Apr 22, ADI 2015 Apr 29, ADI
...	ROXs 42B	... ^a	$1''.14 \pm 0''.004$	$269^\circ 7 \pm 0^\circ 17$	2014 June 8, ADI

^a This system was observed in Y-band.

Table 7
Detected Background Stars in This Study

HD name	Other name	Separation	Position Angle	Date (HST)
36910	CQ Tau	$2''.16 \pm 0''.02$	$53^\circ 1 \pm 0^\circ 5$	2012 Jan
144587	HIP 78996	$3''.49 \pm 0''.01$	$219^\circ 9 \pm 0^\circ 2$	2013 May
148040	HIP 80535	$3''.83 \pm 0''.01$	$175^\circ 8 \pm 0.1$	2015 Apr
169142	...	$2''.21 \pm 0''.01$ $2''.56 \pm 0''.01$ $2''.82 \pm 0''.01$ $2''.96 \pm 0''.01$	$344^\circ 8 \pm 0^\circ 3$ $166^\circ 3 \pm 0^\circ 2$ $14^\circ 1 \pm 0^\circ 2$ $24^\circ 7 \pm 0^\circ 2$	2011 May

5.2. *Preliminary Statistical Discussion Assuming only 2 Companions*

We confirmed 2 convincing low-mass companions at $\sim 100\text{--}150$ AU out of 68 YSOs. The frequency can be simply computed to be $2/68$, corresponding to a probability of $\sim 2.9\%$ for the substellar companions with masses between 1 and $70 M_J$ and projected separations between 50 and 400 AU.

We note that the estimate of the detection frequency of substellar companions is very preliminary, since our calculation ignored several factors needed in the statistical discussion, such as the differences of detection sensitivities and the orbital parameters of companions. To statistically improve these problems in the analysis of the frequency of substellar companions, the Bayesian analysis should be useful (e.g., Brandt et al. 2014a; Biller et al. 2013; Lafrenière et al. 2007). We will describe the statistical framework of Bayesian analysis in the forthcoming paper.

5.3. Comparison with Previous Surveys

5.3.1. Surveys for Nearby Young Stars

Apart from SEEDS, there are some planet-finding programs that targeted more nearby and relatively older targets, such as stars in young moving groups, than those in star forming regions. The Gemini Deep Planet Survey (Lafrenière et al. 2007) observed 85 nearby stars with ages < 6700 Myr and distances < 100 pc. This survey obtained 5σ H -band detection limits of 9.5 mag at $0''.5$, 12.9 at $1''$, 15.0 at $2''$ and 16.5 at $5''$, which are deep enough to detect companions more massive than $2 M_J$ with projected separations ranging from 40 to 200 AU. The Gemini NICI Planet Finding survey (Biller et al. 2013) carried out high contrast imaging of 80 nearby stars with ages younger than several hundreds of Myr. They achieved 5σ completeness detection limit of 10.7, 13.5, and 15.4 mag at $0''.5$, $1''$, and $2''$, which are estimated from 95% threshold of detection limits reported in Biller et al. (2013) by using equation (1) in Brandt et al. (2014a). The VLT/NACO Large Programme (Chauvin et al. 2015) observed solar-type targets with distances smaller than 100 pc and ages younger than 200 Myr, leading to obtain the typical contrasts of ~ 10 , 12, and 13 mag at $0''.5$, $1''$, and $1''.5$, respectively. Other direct imaging surveys for stars older than YSOs ($\sim 10\text{--}5000$ Myr) are also summarized in Chauvin et al. (2015). Our observations targeted YSOs, not nearby young stars, and our results are useful for comparisons with those older than YSOs.

The roughly-estimated probability of substellar companions derived in Section 5.2 can be compared with the probability of previous surveys around older stars. Brandt et al. (2014a) performed a statistical analysis for the high-contrast data taken by the SEEDS and other teams. The statistical analysis for the sample of ~ 250 nearby stars including a lot of young stars in moving groups suggests that 1.0–3.1% (68% confidence) or 0.92–11% (95% confidence) of stars host substellar companions with masses of 5–70 M_J between 10 and 100 AU (Brandt et al. 2014a). Our tentative results look apparently in agreement with this conclusion. The main difference between our study and Brandt et al. (2014a) is the age range and separation range; this difference can be useful for discussing a formation rate of substellar companions and a possibility of their orbital evolutions.

If the statistical analysis for YSOs will result in disagreement with those of older stars such as Brandt et al. (2014a), that disagreement would arise from a difference of conditions in the planet formation or evolution mechanism.

5.3.2. YSO Surveys

Thomas et al. (2007) observed 72 Herbig Ae/Be stars with Gemini/Altair-NIRI and VLT/NACO. In Thomas et al. (2007), some companions including brown dwarfs were detected but gas giant exoplanets were not detected. They achieved K -band detection contrasts of $10^{-2.4}$ at $0''.5$ and 10^{-4} at farther than $2''$; our obtained contrasts are much higher than theirs. The number of our targets is comparable with Thomas et al. (2007). Metchev & Hillenbrand (2009) conducted Paloma/Keck adaptive optics survey around 266 F5-K5 stars between 3 Myr and 3 Gyr and between 10 pc and 190 pc, among which ~ 30 targets are YSOs. They statistically derived the frequency of brown dwarfs ($0.012\text{--}0.072 M_\odot$) to be $3.2^{+3.1}_{-2.7}\%$ (2σ confidence). Fukagawa et al. (2010) observed 16 Herbig Ae/Be stars with Subaru/CIAO and obtained 2σ H -band contrast of ~ 9.5 mag at $2''$ and ~ 12 mag beyond $4''$. SEEDS provides the contrast limits better and more YSO (including T Tauri stars) observations than in Fukagawa et al. (2010). Kraus et al. (2008, 2011) have conducted AO-aided high-resolution imaging surveys at Taurus and Upper Sco with Keck/NIRC2 and Paloma/PHARO observatories to reveal brown dwarf frequency. Typical detection limit of these studies are above the deuterium-burning limit except that the detection limits for some YSOs can constrain an exoplanet with a mass of a few M_J .

As mentioned above, detecting planetary-mass object near YSOs was very difficult due to inadequate contrasts at small separations. Although targets of Kraus et al. (2008, 2011) overlap with ours, this study is the first large scale and systematic exploration for exoplanets around YSOs. Although our detection limits are still ought to be updated, their youth enables to constrain the mass of detectable exoplanet up to a few of jovian mass.

6. SUMMARY

SEEDS project completed main survey of exoplanets and disks around more than 400 targets. Out of these targets, we reduce and analyze the 99 SEEDS/YSO data sets for exoplanet exploration. Our exploration provides the first large-scale and systematical analysis that can achieve high contrast enough to detect young exoplanets, and uses the largest sample among YSO exoplanet survey to the present. YSOs often have protoplanetary disks where planets are being formed. SEEDS project adopts the PDI technique combined with the ADI technique that are effective to detect both the disks and exoplanets around YSOs.

We discovered 15 new point sources within 400 AU around 68 YSOs; among those, 7 are identified to be background stars, one is identified to be a stellar companion, and one is either a stellar companion or background star. We will aim at follow-up observations of remaining 6 companion candidates to conduct their CPM tests. We also confirmed 2 companions which are previously reported; GQ Lup b and ROXs 42B b. LKCa 15 b, c

and HD169142 b are not detected in this research. We estimated 5σ detection limits of contrast as a function of separation angle, which are transformed into detection limits in mass based on the properties of the observed YSOs (see Table 5) and the COND03 models. As a result, we typically achieved contrasts of $\sim 10^{-3.5}$ at $0''.5$, 10^{-4} – 10^{-5} at $1''$, and $10^{-4.5}$ – 10^{-6} beyond $2''$. We can also determine typical upper limits of potentially existing exoplanets to be $\sim 10 M_J$ at $0''.5$ and $\sim 6 M_J$ at $1''$.

Since previous studies calculated older-exoplanet frequency than our work (e.g. Brandt et al. 2014a; Chauvin et al. 2015), our study will help compare the results of imaging surveys that targeted different ages.

Furthermore, we expect the next ‘extreme’ adaptive optics system such as Gemini/GPI (Macintosh et al. 2006), VLT/SPHERE (Beuzit et al. 2006), and SCExAO (Guyon et al. 2010) to reveal a relationship between giant exoplanets and disk feature exploring the gap region in protoplanetary disks.

The authors thank David Lafrenière for generously providing the source code for the LOCI algorithm. The authors would like to thank the anonymous referees for their constructive comments and suggestions to improve the quality of the paper. This research is based on data collected at the Subaru Telescope, which is operated by the National Astronomical Observatories of Japan. Based in part on data collected at Subaru telescope and obtained from the SMOKA, which is operated by the Astronomy Data Center, National Astronomical Observatory of Japan. We also acknowledge the SDPS project for our use of the CIAO archival data. Some/all of the data presented in this paper were obtained from the Mikulski Archive for Space Telescopes (MAST). STScI is operated by the Association of Universities for Research in Astronomy, Inc., under NASA contract NAS5-26555. Support for MAST for non-HST data is provided by the NASA Office of Space Science via grant NNX09AF08G and by other grants and contracts. Data analysis were carried out on common use data analysis computer system at the Astronomy Data Center, ADC, of the National Astronomical Observatory of Japan. This research has made use of NASA’s Astrophysics Data System Bibliographic Services. This research has made use of the SIMBAD database, operated at CDS, Strasbourg, France. This research has made use of the VizieR catalogue access tool, CDS, Strasbourg, France. The original description of the VizieR service was published in *A&AS* 143, 23. This publication makes use of data products from the Two Micron All Sky Survey, which is a joint project of the University of Massachusetts and the Infrared Processing and Analysis Center/California Institute of Technology, funded by the National Aeronautics and Space Administration and the National Science Foundation.

MK was supported by Japan Society for Promotion of Science (JSPS) Fellowship for Research and this work was partially supported by the Grant-in-Aid for JSPS Fellows (Grant Number 25-8826). JC is supported by the U.S. National Science Foundation under Award No. 1009203. MT is partly supported by the JSPS Grant-in-Aid (Nos. 15H02063 and 22000005).

The authors wish to recognize and acknowledge the very significant cultural role and reverence that the sum-

mit of Mauna Kea has always had within the indigenous Hawaiian community. We are most fortunate to have the opportunity to conduct observations from this mountain.

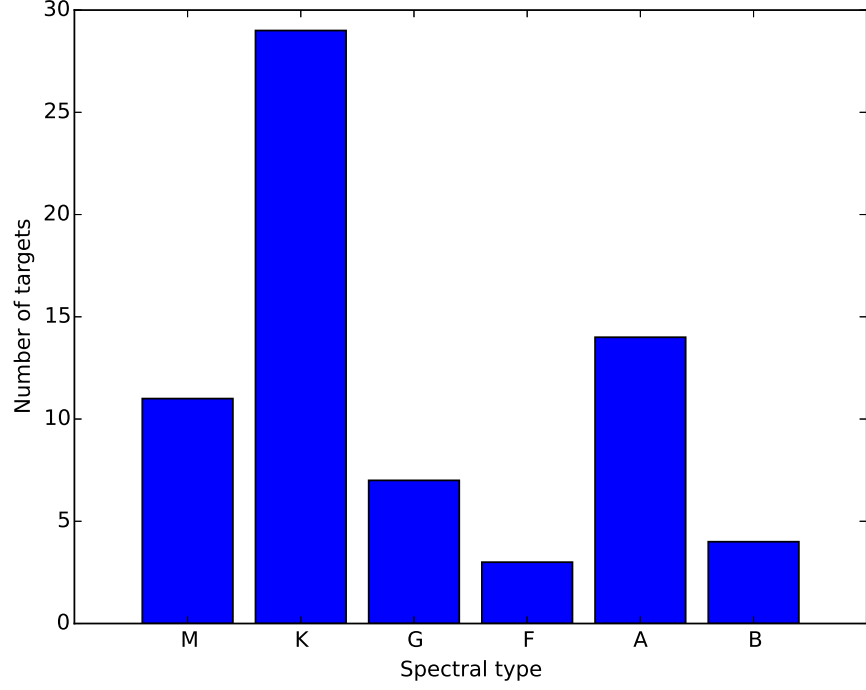


Figure 8. Distribution of spectral types of YSOs that we targeted in this work.

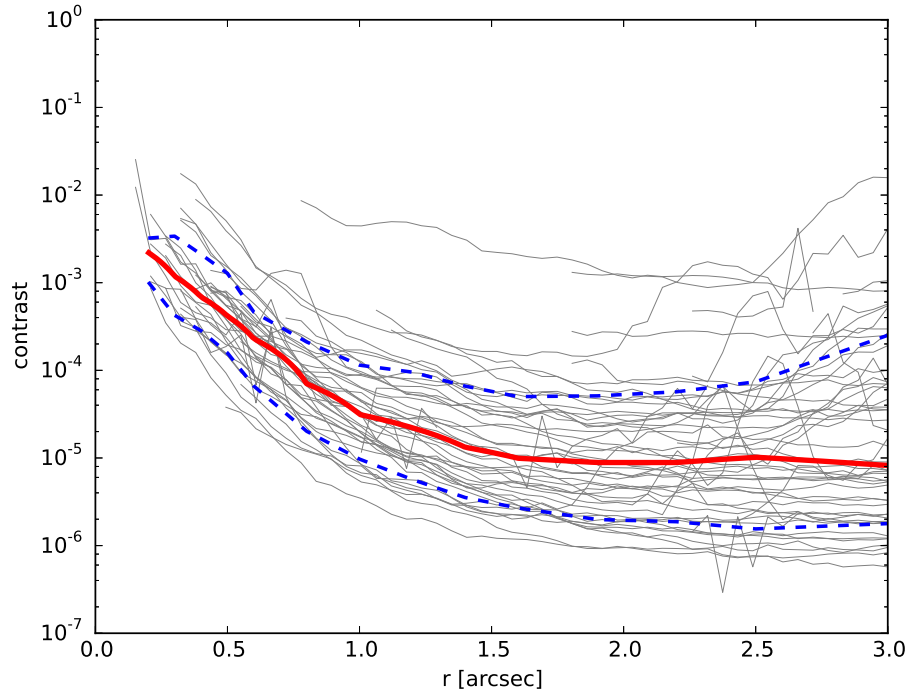


Figure 9. Radial profile of contrast curves that are brighter than 8 mag in H or K_s band (gray); the red line represents their median contrast curve and the two blue dashed lines represent 1σ range. The horizontal axis represents a separation in arcsec and the vertical axis is a contrast to the central star. We do not show contrast curves further than $3''$ because of the qPDI limitation.

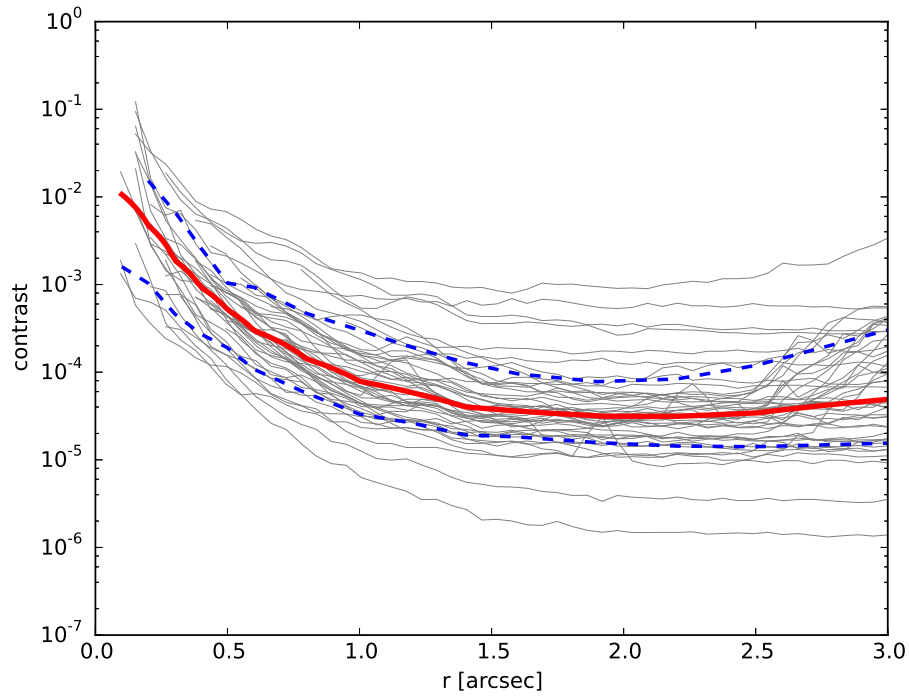


Figure 10. Same as Figure 9 except that our targets' brightness magnitudes at the observed band are not brighter than 8 mag.

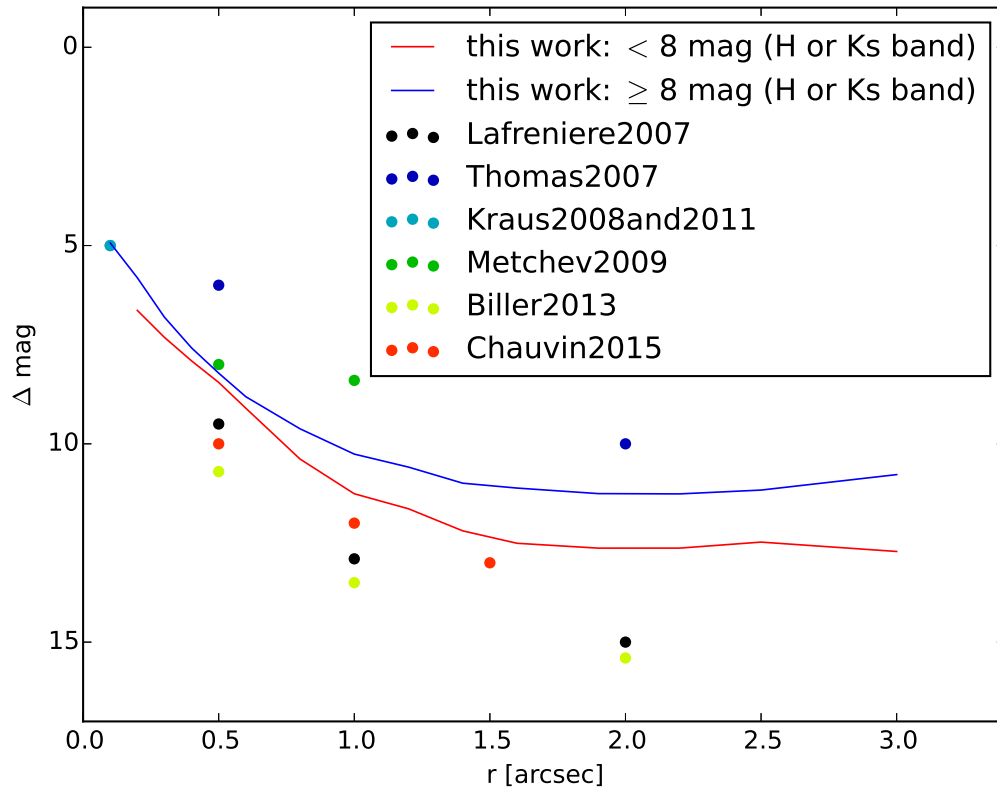


Figure 11. Comparing typical contrast limits between this work and the other YSO and moving group surveys. The studies labeled in this Figure are described in Section 5.3. We roughly investigated plots by checking contrast curves in each study.

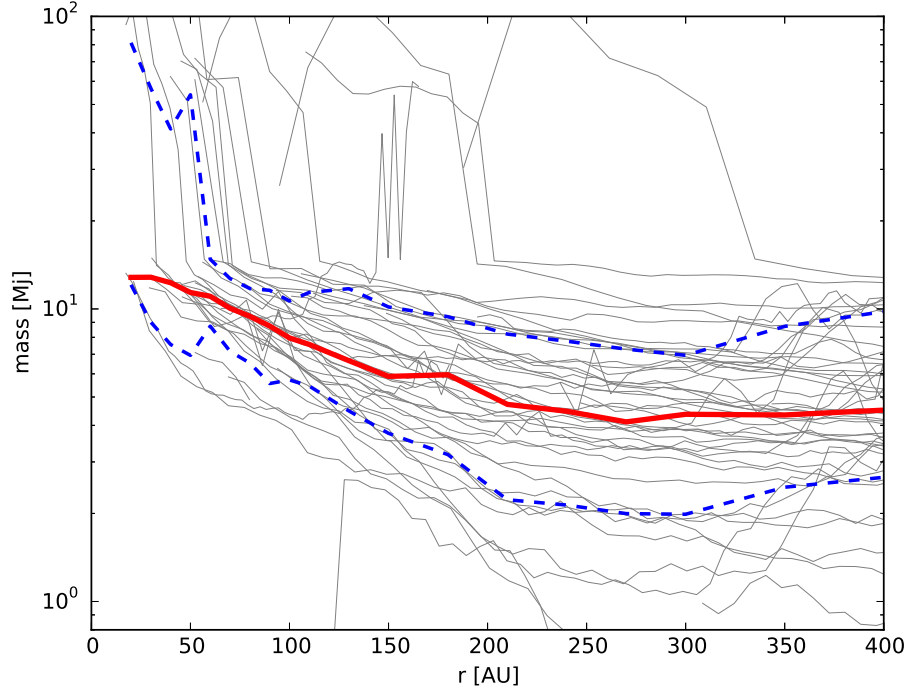


Figure 12. Detection limits of each YSO in unit of mass. These gray lines are converted from the results in Figure 9 using COND03 model (Baraffe et al. 2003). The median value of the detection limits is represented by the red line and the 1σ range is showed by the blue dashed lines. The vertical and horizontal axes represent the mass of 5σ detection limit and the separation in AU, respectively.

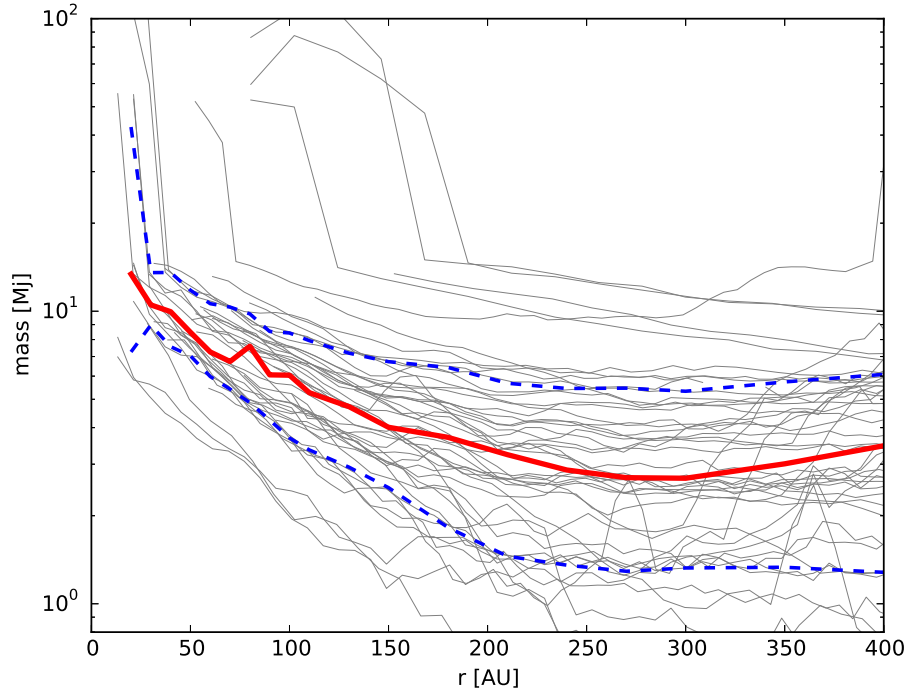


Figure 13. Same as Figure 12 except that lines are converted from those in Figure 10.

REFERENCES

- Akiyama, E., Hasegawa, Y., Hayashi, M., & Iguchi, S. 2016, *ApJ*, 818, 158
- Akiyama, E., Momose, M., Kitamura, Y., et al. 2013, *PASJ*, 65, doi:10.1093/pasj/65.6.123
- Akiyama, E., Muto, T., Kusakabe, N., et al. 2015, *ApJ*, 802, L17
- Alecian, E., Wade, G. A., Catala, C., et al. 2013, *MNRAS*, 429, 1001
- Allard, F., Homeier, D., & Freytag, B. 2011, in *Astronomical Society of the Pacific Conference Series*, Vol. 448, 16th Cambridge Workshop on Cool Stars, Stellar Systems, and the Sun, ed. C. Johns-Krull, M. K. Browning, & A. A. West, 91
- Allen, L. E., Myers, P. C., Di Francesco, J., et al. 2002, *ApJ*, 566, 993
- ALMA Partnership, Brogan, C. L., Pérez, L. M., et al. 2015, *ApJL*, 808, L3
- Andre, P., & Montmerle, T. 1994, *ApJ*, 420, 837
- Andrews, S. M., Hughes, A. M., Wilner, D. J., & Qi, C. 2008, *ApJ*, 678, L133
- Andrews, S. M., Rosenfeld, K. A., Kraus, A. L., & Wilner, D. J. 2013, *ApJ*, 771, 129
- Andrews, S. M., & Williams, J. P. 2005, *ApJ*, 631, 1134
- . 2007, *ApJ*, 659, 705
- Andrews, S. M., Wilner, D. J., Espaillat, C., et al. 2011, *ApJ*, 732, 42
- Andrews, S. M., Wilner, D. J., Hughes, A. M., Qi, C., & Dullemond, C. P. 2009, *ApJ*, 700, 1502
- Ansdell, M., Gaidos, E., Rappaport, S. A., et al. 2016, *ApJ*, 816, 69
- Augereau, J. C., Lagrange, A. M., Mouillet, D., & Ménard, F. 2001, *A&A*, 365, 78
- Auvergne, M., Bodin, P., Boissard, L., et al. 2009, *A&A*, 506, 411
- Avenhaus, H., Quanz, S. P., Schmid, H. M., et al. 2014, *ApJ*, 781, 87
- Bailey, V., Meshkat, T., Reiter, M., et al. 2014, *ApJL*, 780, L4
- Balachandran, S. 1990, *ApJ*, 354, 310
- Baraffe, I., Chabrier, G., Allard, F., & Hauschildt, P. H. 1998, *A&A*, 337, 403
- Baraffe, I., Chabrier, G., Barman, T., Allard, F., & Hauschildt, P. H. 2003, *A&A*, 712, 14
- Barsony, M., Koresko, C., & Matthews, K. 2003, *ApJ*, 591, 1064
- Batalha, N. M., Borucki, W. J., Bryson, S. T., et al. 2011, *ApJ*, 729, 27
- Beckwith, S. V. W., Sargent, A. I., Chini, R. S., & Guesten, R. 1990, *AJ*, 99, 924
- Benisty, M., Juhasz, A., Boccaletti, A., et al. 2015, *A&A*, 578, L6
- Bertout, C., Robichon, N., & Arenou, F. 1999, *A&A*, 352, 574
- Bertout, C., Siess, L., & Cabrit, S. 2007, *A&A*, 473, L21
- Beuzit, J.-L., Feldt, M., Dohlen, K., et al. 2006, *The Messenger*, 125, 29
- Biller, B., Lacour, S., Juhász, A., et al. 2012, *ApJL*, 753, L38
- Biller, B. A., Liu, M. C., Wahhaj, Z., et al. 2013, *ApJ*, 777, 160
- Blandford, R. D., & Payne, D. G. 1982, *MNRAS*, 199, 883
- Bouvier, J., & Appenzeller, I. 1992, *A&AS*, 92, 481
- Brandt, T. D., McElwain, M. W., Turner, E. L., et al. 2013, *ApJ*, 764, 183
- . 2014a, *ApJ*, 794, 159
- Brandt, T. D., Kuzuhara, M., McElwain, M. W., et al. 2014b, *ApJ*, 786, 1
- Brown, J. M., Blake, G. A., Qi, C., Dullemond, C. P., & Wilner, D. J. 2008, *ApJL*, 675, L109
- Brown, J. M., Blake, G. A., Qi, C., et al. 2009, *ApJ*, 704, 496
- Brown, J. M., Herczeg, G. J., Pontoppidan, K. M., & van Dishoeck, E. F. 2012, *ApJ*, 744, 116
- Brown, J. M., Blake, G. A., Dullemond, C. P., et al. 2007, *ApJL*, 664, L107
- Bustamante, I., Merín, B., Ribas, Á., et al. 2015, *A&A*, 578, A23
- Caballero, J. A. 2010, *A&A*, 511, L9
- Caballero, J. A., & Solano, E. 2008, *A&A*, 485, 931
- Calvet, N., D'Alessio, P., Hartmann, L., et al. 2002, *ApJ*, 568, 1008
- Calvet, N., D'Alessio, P., Watson, D. M., et al. 2005, *ApJL*, 630, L185
- Cardelli, J. A., Clayton, G. C., & Mathis, J. S. 1989, *ApJ*, 345, 245
- Carpenter, J. M., Mamajek, E. E., Hillenbrand, L. A., & Meyer, M. R. 2006, *ApJL*, 651, L49
- . 2009, *ApJ*, 705, 1646
- Carpenter, J. M., Ricci, L., & Isella, A. 2014, *ApJ*, 787, 42
- Carson, J., Thalmann, C., Janson, M., et al. 2013, *ApJL*, 763, L32
- Chapillon, E., Parise, B., Guilloteau, S., Dutrey, A., & Wakelam, V. 2010, *A&A*, 520, A61
- Chauvin, G., Lagrange, A.-M., Beust, H., et al. 2012, *A&A*, 542, A41
- Chauvin, G., Vigan, A., Bonnefoy, M., et al. 2015, *A&A*, 573, A127
- Chen, C. H., Jura, M., Gordon, K. D., & Blaylock, M. 2005, *ApJ*, 623, 493
- Chen, C. H., Mamajek, E. E., Bitner, M. A., et al. 2011, *ApJ*, 738, 122
- Chini, R., Kämpgen, K., Reipurth, B., et al. 2003, *A&A*, 409, 235
- Cieza, L., Padgett, D. L., Stapelfeldt, K. R., et al. 2007, *ApJ*, 667, 308
- Cieza, L. A., Schreiber, M. R., Romero, G. A., et al. 2010, *ApJ*, 712, 925
- Cieza, L. A., Mathews, G. S., Williams, J. P., et al. 2012, *ApJ*, 752, 75
- Comerón, F. 2008, *The Lupus Clouds*, ed. B. Reipurth, 295
- Comerón, F., Spezzi, L., & López Martí, B. 2009, *A&A*, 500, 1045
- Costigan, G., Vink, J. S., Scholz, A., Ray, T., & Testi, L. 2014, *MNRAS*, 440, 3444
- Currie, T., Burrows, A., & Daemgen, S. 2014a, *ApJ*, 787, 104
- Currie, T., Cloutier, R., Brittain, S., et al. 2015, *ApJL*, 814, L27
- Currie, T., Daemgen, S., Debes, J., et al. 2014b, *ApJ*, 780, L30
- Currie, T., Burrows, A., Itoh, Y., et al. 2011, *ApJ*, 729, 128
- Currie, T., Muto, T., Kudo, T., et al. 2014c, *ApJL*, 796, L30
- Cutri, R. M., Skrutskie, M. F., van Dyk, S., et al. 2003, *VizieR Online Data Catalog*, 2246
- Dahm, S. E. 2010, *AJ*, 140, 1444
- Dahm, S. E., & Carpenter, J. M. 2009, *ApJ*, 137, 4024
- Dahm, S. E., Slesnick, C. L., & White, R. J. 2012, *ApJ*, 745, 56
- Dai, Y., Wilner, D. J., Andrews, S. M., & Ohashi, N. 2010, *AJ*, 139, 626
- D'Antona, F., & Mazzitelli, I. 1994, *ApJS*, 90, 467
- de Leon, J., Takami, M., Karr, J. L., et al. 2015, *ApJL*, 806, L10
- de Zeeuw, P. T., Hoogerwerf, R., de Bruijne, J. H. J., Brown, A. G. A., & Blaauw, A. 1999, *AJ*, 117, 354
- Debes, J. H., Jang-Condell, H., Weinberger, A. J., Roberge, A., & Schneider, G. 2013, *ApJ*, 771, 45
- Dent, W. R. F., Greaves, J. S., & Coulson, I. M. 2005, *MNRAS*, 359, 663
- Dent, W. R. F., Torrelles, J. M., Osorio, M., Calvet, N., & Anglada, G. 2006, *MNRAS*, 365, 1283
- Dent, W. R. F., Thi, W. F., Kamp, I., et al. 2013, *PASP*, 125, 477
- Dodson-Robinson, S. E., Veras, D., Ford, E. B., & Beichman, C. A. 2009, *ApJ*, 707, 79
- Dong, R., Zhu, Z., Rafikov, R. R., & Stone, J. M. 2015, *ApJL*, 809, L5
- Doucet, C., Pantin, E., Lagage, P. O., & Dullemond, C. P. 2006, *A&A*, 460, 117
- Drew, J. E., Busfield, G., Hoare, M. G., et al. 1997, *MNRAS*, 286, 538
- Dunham, M. M., Allen, L. E., Evans, II, N. J., et al. 2015, *ApJ*, 220, 11
- Dunkin, S. K., Barlow, M. J., & Ryan, S. G. 1997, *MNRAS*, 286, 604
- Dutrey, A., Guilloteau, S., & Simon, M. 2003, *A&A*, 402, 1003
- Egner, S., Ikeda, Y., Watanabe, M., et al. 2010, in *Proc. SPIE*, Vol. 7736, 4
- Elia, D., Strafella, F., Campeggio, L., et al. 2004, *ApJ*, 601, 1000
- Elliott, P., Huélamo, N., Bouy, H., et al. 2015, *A&A*, 580, A88
- ESA, ed. 1997, *ESA Special Publication*, Vol. 1200, *The HIPPARCOS and TYCHO catalogues. Astrometric and photometric star catalogues derived from the ESA HIPPARCOS Space Astrometry Mission*
- Espaillat, C., Andrews, S., Powell, D., et al. 2015, *ApJ*, 807, 156
- Espaillat, C., Calvet, N., D'Alessio, P., et al. 2007, *ApJL*, 670, L135
- Espaillat, C., Furlan, E., D'Alessio, P., et al. 2011, *ApJ*, 728, 49
- Espaillat, C., D'Alessio, P., Hernández, J., et al. 2010, *ApJ*, 717, 441

- Espaillet, C., Muzerolle, J., Najita, J., et al. 2014, *Protostars and Planets VI*, 497
- Fernandez, M., Ortiz, E., Eiroa, C., & Miranda, L. F. 1995, *A&AS*, 114, 439
- Follette, K. B., Tamura, M., Hashimoto, J., et al. 2013, *ApJ*, 767, 10
- Forbrich, J., & Preibisch, T. 2007, *A&A*, 475, 959
- France, K., Schindhelm, E., Herczeg, G. J., et al. 2012, *ApJ*, 756, 171
- Fukagawa, M., Tamura, M., Itoh, Y., et al. 2006, *ApJL*, 636, L153
- Fukagawa, M., Hayashi, M., Tamura, M., et al. 2004, *ApJL*, 605, L53
- Fukagawa, M., Tamura, M., Itoh, Y., et al. 2010, *PASJ*, 62, 347
- Fukagawa, M., Tsukagoshi, T., Momose, M., et al. 2013, *PASJ*, 65, L14
- Furlan, E., Hartmann, L., Calvet, N., et al. 2006, *ApJS*, 165, 568
- Furlan, E., Watson, D. M., McClure, M. K., et al. 2009, *ApJ*, 703, 1964
- Goto, M., Carmona, A., Linz, H., et al. 2012, *ApJ*, 748, 6
- Grady, C. A., Schneider, G., Hamaguchi, K., et al. 2007, *ApJ*, 665, 1391
- Grady, C. A., Hamaguchi, K., Schneider, G., et al. 2010, *ApJ*, 719, 1565
- Grady, C. A., Muto, T., Hashimoto, J., et al. 2013, *ApJ*, 762, 48
- Greene, T. P., & Meyer, M. R. 1995, *ApJ*, 450, 233
- Gregorio-Hetem, J., & Hetem, A. 2002, *MNRAS*, 336, 197
- Guillout, P., Frasca, A., Klutsch, A., Marilli, E., & Montes, D. 2010, *A&A*, 520, A94
- Gullbring, E., Hartmann, L., Briceño, C., & Calvet, N. 1998, *ApJ*, 492, 323
- Guyon, O., Martinache, F., Garrel, V., et al. 2010, in *Society of Photo-Optical Instrumentation Engineers (SPIE) Conference Series*, Vol. 7736, *Society of Photo-Optical Instrumentation Engineers (SPIE) Conference Series*, 24
- Hartmann, L., Calvet, N., Gullbring, E., & D'Alessio, P. 1998, *ApJ*, 495, 385
- Hartmann, L., Megeath, S. T., Allen, L., et al. 2005, *ApJ*, 629, 881
- Hashimoto, J., Tamura, M., Muto, T., et al. 2011, *ApJ*, 729, L17
- Hashimoto, J., Dong, R., Kudo, T., et al. 2012, *ApJ*, 758, L19
- Hayano, Y., Takami, H., Guyon, O., et al. 2008, in *Society of Photo-Optical Instrumentation Engineers (SPIE) Conference Series*, Vol. 7015, *Society of Photo-Optical Instrumentation Engineers (SPIE) Conference Series*, 10
- Hayashi, C., Nakazawa, K., & Nakagawa, Y. 1985, 1100
- Herczeg, G. J., & Hillenbrand, L. A. 2014, *ApJ*, 786, 97
- Herczeg, G. J., Wood, B. E., Linsky, J. L., Valenti, J. A., & Johns-Krull, C. M. 2004, *ApJ*, 607, 369
- Hernández, J., Calvet, N., Briceño, C., Hartmann, L., & Berlind, P. 2004, *ApJ*, 127, 1682
- Hernández, J., Calvet, N., Hartmann, L., et al. 2005, *AJ*, 129, 856
- Hillenbrand, L. A., Strom, S. E., Vrba, F. J., & Keene, J. 1992, *ApJ*, 397, 613
- Hog, E., Kuzmin, A., Bastian, U., et al. 1998, *A&A*, 335, L65
- Høg, E., Fabricius, C., Makarov, V. V., et al. 2000, *A&A*, 355, L27
- Hogerheijde, M. R., van Langevelde, H. J., Mundy, L. G., Blake, G. A., & van Dishoeck, E. F. 1997, *ApJL*, 490, L99
- Holman, M., Touma, J., & Tremaine, S. 1997, *Nature*, 386, 254
- Houk, N. 1978, *Michigan catalogue of two-dimensional spectral types for the HD stars*
- . 1982, *Michigan Catalogue of Two-dimensional Spectral Types for the HD stars. Volume 3. Declinations -40°0 to -26°0*.
- Houk, N., & Smith-Moore, M. 1988, *Michigan Catalogue of Two-dimensional Spectral Types for the HD Stars. Volume 4, Declinations -26°0 to -12°0*.
- Howard, C. D., Sandell, G., Vacca, W. D., et al. 2013, *ApJ*, 776, 21
- Hughes, A. M., Andrews, S. M., Espaillat, C., et al. 2009, *ApJ*, 698, 131
- Hughes, A. M., Andrews, S. M., Wilner, D. J., et al. 2010, *AJ*, 140, 887
- Hughes, J., Hartigan, P., & Clampitt, L. 1993, *AJ*, 105, 571
- Hughes, J., Hartigan, P., Krautter, J., & Kelemen, J. 1994, *AJ*, 108, 1071
- Ida, S., Lin, D. N. C., & Nagasawa, M. 2013, *ApJ*, 775, 42
- Ingleby, L., Espaillat, C., Calvet, N., et al. 2015, *ApJ*, 805, 149
- Isella, A., Carpenter, J. M., & Sargent, A. I. 2010a, *ApJ*, 714, 1746
- Isella, A., Natta, A., Wilner, D., Carpenter, J. M., & Testi, L. 2010b, *ApJ*, 725, 1735
- Isella, A., Pérez, L. M., Carpenter, J. M., et al. 2013, *ApJ*, 775, 30
- Itoh, Y., Hayashi, M., Tamura, M., et al. 2005, *ApJ*, 620, 984
- Itoh, Y., Oasa, Y., Kudo, T., et al. 2014, *Research in A&A*, 14, 1438
- Jang-Condell, H., & Turner, N. J. 2012, *ApJ*, 749, 153
- Janson, M., Brandt, T. D., Moro-Martín, A., et al. 2013, *ApJ*, 773, 73
- Joergens, V., Guenther, E., Neuhäuser, R., Fernández, M., & Vijapurkar, J. 2001, *A&A*, 373, 966
- Joy, A. H. 1945, *ApJ*, 102, 168
- Kaas, A. A., Olofsson, G., Bontemps, S., et al. 2004, *A&A*, 421, 623
- Karr, J. L., Ohashi, N., Kudo, T., & Tamura, M. 2010, *AJ*, 139, 1015
- Kenyon, S. J., Gómez, M., & Whitney, B. A. 2008, *Low Mass Star Formation in the Taurus-Auriga Clouds*, 405
- Kenyon, S. J., & Hartmann, L. 1995a, *ApJS*, 101, 117
- . 1995b, *ApJ*, 101, 117
- Kenyon, S. J., Hartmann, L. W., Strom, K. M., & Strom, S. E. 1990, *AJ*, 99, 869
- Khalafinejad, S., Maaskant, K. M., Mariñas, N., & Tielens, A. G. G. M. 2016, *A&A*, 587, A62
- Kim, K. H., Watson, D. M., Manoj, P., et al. 2013, *ApJ*, 769, 149
- Kitamura, Y., Momose, M., Yokogawa, S., et al. 2002, *ApJ*, 581, 357
- Knacke, R. F., Strom, K. M., Strom, S. E., Young, E., & Kunkel, W. 1973, *ApJ*, 179, 847
- Köhler, R., Kunkel, M., Leinert, C., & Zinnecker, H. 2000a, *A&A*, 356, 541
- . 2000b, *A&A*, 356, 541
- Köhler, R., Neuhäuser, R., Krämer, S., et al. 2008, *A&A*, 488, 997
- Kokubo, E., & Ida, S. 2002, *ApJ*, 581, 666
- Kratter, K. M., Matzner, C. D., Krumholz, M. R., & Klein, R. I. 2010, *ApJ*, 708, 1585
- Kraus, A. L., & Hillenbrand, L. A. 2009, *ApJ*, 704, 531
- Kraus, A. L., & Ireland, M. J. 2012, *ApJ*, 745, 5
- Kraus, A. L., Ireland, M. J., Cieza, L. A., et al. 2014, *ApJ*, 781, 20
- Kraus, A. L., Ireland, M. J., Martinache, F., & Hillenbrand, L. A. 2011, *ApJ*, 731, 8
- Kraus, A. L., Ireland, M. J., Martinache, F., & Lloyd, J. P. 2008, *ApJ*, 679, 762
- Kraus, S., Ireland, M. J., Sitko, M. L., et al. 2013, *ApJ*, 768, 80
- Krist, J. E., Stapelfeldt, K. R., Ménard, F., Padgett, D. L., & Burrows, C. J. 2000, *ApJ*, 538, 793
- Krist, J. E., Stapelfeldt, K. R., Golimowski, D. A., et al. 2005, *AJ*, 130, 2778
- Küçük, I., & Akkaya, I. 2010, *RMXAA*, 46, 109
- Kuhn, J. R., Wu, Z., & Poenie, M. 2001, *Biophysical journal*, 80, 972
- Kusakabe, N., Grady, C. A., Sitko, M. L., et al. 2012, *ApJ*, 753, 153
- Kuzuhara, M. 2016, in prep.
- Kuzuhara, M., Tamura, M., Kudo, T., et al. 2013, *ApJ*, 774, 11
- Lafreniere, D., Marois, C., Doyon, R., Nadeau, D., & Artigau, E. 2007, *ApJ*, 660, 770
- Lafreniere, D., Doyon, R., Marois, C., et al. 2007, *ApJ*, 670, 1367
- Lagrange, A.-M., Bonnefoy, M., Chauvin, G., et al. 2010, *Science*, 329, 57
- Lavigne, J.-F., Doyon, R., Lafreniere, D., Marois, C., & Barman, T. 2009, *ApJ*, 704, 1098
- Leinert, C., Zinnecker, H., Weitzel, N., et al. 1993, *A&A*, 278, 129
- Li, W., Evans, II, N. J., Harvey, P. M., & Colome, C. 1994, *ApJ*, 433, 199
- Liu, W. M., Hinz, P. M., Meyer, M. R., et al. 2007, *ApJ*, 658, 1164
- Lombardi, M., Lada, C. J., & Alves, J. 2008, *A&A*, 480, 785
- López-Martínez, F., & Gómez de Castro, A. I. 2015, *MNRAS*, 448, 484
- Luhman, K. L., Allen, P. R., Espaillat, C., Hartmann, L., & Calvet, N. 2010, *ApJS*, 186, 111
- Luhman, K. L., Mamajek, E. E., Allen, P. R., Muench, A. A., & Finkbeiner, D. P. 2009, *ApJ*, 691, 1265
- Luhman, K. L., & Rieke, G. H. 1999, *ApJ*, 525, 440
- Lynch, C., Mutel, R. L., Güdel, M., et al. 2013, *ApJ*, 766, 53

- Macintosh, B., Graham, J., Palmer, D., et al. 2006, in Society of Photo-Optical Instrumentation Engineers (SPIE) Conference Series, Vol. 6272, Society of Photo-Optical Instrumentation Engineers (SPIE) Conference Series, 0
- Magazzu, A., Rebolo, R., & Pavlenko, I. V. 1992, *ApJ*, 392, 159
- Makarov, V. V. 2007, *ApJ*, 670, 1225
- Malbet, F., Benisty, M., de Wit, W.-J., et al. 2007, *A&A*, 464, 43
- Malfait, K., Bogaert, E., & Waelkens, C. 1998, *A&A*, 331, 211
- Marleau, G.-D., & Cumming, A. 2014, *MNRAS*, 437, 1378
- Marley, M. S., Fortney, J. J., Hubickyj, O., Bodenheimer, P., & Lissauer, J. J. 2007, *ApJ*, 655, 541
- Marois, C., Lafreniere, D., Doyon, R., Macintosh, B., & Nadeau, D. 2006, *ApJ*, 641, 556
- Marois, C., Macintosh, B., Barman, T., et al. 2008, *Science*, 322, 1348
- Marsh, K. A., & Mahoney, M. J. 1992, *ApJ*, 395, L115
- . 1993, *ApJ*, 405, L71
- Martin, E. L., Montmerle, T., Gregorio-Hetem, J., & Casanova, S. 1998, *MNRAS*, 300, 733
- Martin, E. L., Rebolo, R., Magazzu, A., & Pavlenko, Y. V. 1994, *A&A*, 282, 503
- Mathews, G. S., Pinte, C., Duchêne, G., Williams, J. P., & Ménard, F. 2013, *A&A*, 558, A66
- Mathews, G. S., Williams, J. P., & Ménard, F. 2012, *ApJ*, 753, 59
- Matter, A., Labadie, L., Kreplin, A., et al. 2014, *A&A*, 561, A26
- Mawet, D., Absil, O., Montagnier, G., et al. 2012, *A&A*, 544, A131
- Mayama, S., Hashimoto, J., Muto, T., et al. 2012, *ApJ*, 760, L26
- Mayor, M., & Queloz, D. 1995, */nat*, 378, 355
- McCabe, C., Ghez, A. M., Prato, L., et al. 2006, *ApJ*, 636, 932
- McClure, M. K., Furlan, E., Manoj, P., et al. 2010, *ApJ*, 188, 75
- McElwain, M. W., Metchev, S. A., Larkin, J. E., et al. 2007, *ApJ*, 656, 505
- Meeus, G., Waelkens, C., & Malfait, K. 1998, *A&A*, 329, 131
- Meeus, G., Montesinos, B., Mendigutía, I., et al. 2012, *A&A*, 544, A78
- Melo, C. H. F. 2003, *A&A*, 410, 269
- Mendigutía, I., Fairlamb, J., Montesinos, B., et al. 2014, *ApJ*, 790, 21
- Menu, J., van Boekel, R., Henning, T., et al. 2014, *A&A*, 564, A93
- Merín, B., Montesinos, B., Eiroa, C., et al. 2004, *A&A*, 419, 301
- Merín, B., Jørgensen, J., Spezzi, L., et al. 2008, *ApJS*, 177, 551
- Metchev, S. A., & Hillenbrand, L. A. 2009, *ApJS*, 181, 62
- Metchev, S. A., Hillenbrand, L. A., & Meyer, M. R. 2004, *ApJ*, 600, 435
- Millan-Gabet, R., Schloerb, F. P., & Traub, W. A. 2001, *ApJ*, 546, 358
- Moffat, A. F. J. 1969, *A&A*, 3, 455
- Momose, M., Morita, A., Fukagawa, M., et al. 2015, *PASJ*, 67, 83
- Monet, D. G., Levine, S. E., Canzian, B., et al. 2003, *AJ*, 125, 984
- Monnier, J. D., Tannirkulam, A., Tuthill, P. G., et al. 2008, *ApJL*, 681, L97
- Montesinos, B., Eiroa, C., Mora, A., & Merín, B. 2009, *A&A*, 495, 901
- Moór, A., Ábrahám, P., Derekas, A., et al. 2006, *ApJ*, 644, 525
- Moór, A., Juhász, A., Kóspál, Á., et al. 2013, *ApJ*, 777, L25
- Mora, A., Merín, B., Solano, E., et al. 2001, *A&A*, 378, 116
- Müller, A., van den Ancker, M. E., Launhardt, R., et al. 2011, *A&A*, 530, A85
- Murakawa, K., Oya, S., Pyo, T.-S., & Ishii, M. 2008, *A&A*, 492, 731
- Muto, T., Grady, C. A., Hashimoto, J., et al. 2012, *ApJ*, 748, L22
- Najita, J. R., Strom, S. E., & Muzerolle, J. 2007, *MNRAS*, 378, 369
- Nakajima, T., & Golimowski, D. A. 1995, *AJ*, 109, 1181
- Naud, M.-E., Artigau, É., Malo, L., et al. 2014, *ApJ*, 787, 5
- Neuhäuser, R., Guenther, E. W., Wuchterl, G., et al. 2005, *A&A*, 435, L13
- Neuhäuser, R., Mugrauer, M., Seifahrt, A., Schmidt, T. O. B., & Vogt, N. 2008, *A&A*, 484, 281
- Neuhäuser, R., Walter, F. M., Covino, E., et al. 2000, *A&ASupplement*, 146, 323
- Nuernberger, D., Chini, R., & Zinnecker, H. 1997, *A&A*, 324, 1036
- Okamoto, Y. K., Kataza, H., Honda, M., et al. 2009, *ApJ*, 706, 665
- Oppenheimer, B. R., Brenner, D., Hinkley, S., et al. 2008, *ApJ*, 679, 1574
- Orellana, M., Cieza, L. A., Schreiber, M. R., et al. 2012, *A&A*, 539, A41
- Padgett, D. L., Cieza, L., Stapelfeldt, K. R., et al. 2006, *ApJ*, 645, 1283
- Panić, O., & Hogerheijde, M. R. 2009, *Astronomy and Astrophysics*, 508, 707
- Panić, O., Hogerheijde, M. R., Wilner, D., & Qi, C. 2009, *A&A*, 501, 269
- Pecaut, M. J., & Mamajek, E. E. 2013, *ApJS*, 208, 9
- Pecaut, M. J., Mamajek, E. E., & Bubar, E. J. 2012, *ApJ*, 746, 154
- Pérez, L. M., Isella, A., Carpenter, J. M., & Chandler, C. J. 2014, *ApJ*, 783, L13
- Perrin, M. D., Schneider, G., Duchene, G., et al. 2009, *ApJL*, 707, L132
- Piétu, V., Dutrey, A., Guilloteau, S., Chapillon, E., & Pety, J. 2006, *A&A*, 460, L43
- Piétu, V., Dutrey, A., & Kahane, C. 2003, *A&A*, 398, 565
- Pinte, C., Padgett, D. L., Ménard, F., et al. 2008, *A&A*, 489, 633
- Prato, L., Greene, T. P., & Simon, M. 2003, *ApJ*, 584, 853
- Preibisch, T., Guenther, E., Zinnecker, H., et al. 1998, *A&A*, 333, 619
- Preibisch, T., & Zinnecker, H. 1999, *AJ*, 117, 2381
- Qi, C., Ho, P. T. P., Wilner, D. J., et al. 2004, *ApJL*, 616, L11
- Quanz, S. P., Amara, A., Meyer, M. R., et al. 2013a, *ApJ*, 766, L1
- Quanz, S. P., Avenhaus, H., Buenzli, E., et al. 2013b, *ApJL*, 766, L2
- Ratzka, T., Köhler, R., & Leinert, C. 2005, *A&A*, 437, 611
- Ratzka, T., Schegerer, A. A., Leinert, C., et al. 2009, *A&A*, 502, 623
- Rebull, L. M., Padgett, D. L., McCabe, C.-E., et al. 2010, *ApJ*, 186, 259
- Rebull, L. M., Koenig, X. P., Padgett, D. L., et al. 2011, *ApJS*, 196, 4
- Reggiani, M., Quanz, S. P., Meyer, M. R., et al. 2014, *ApJL*, 792, L23
- Riaud, P., Mawet, D., Absil, O., et al. 2006, *A&A*, 458, 317
- Ricci, L., Testi, L., Natta, A., et al. 2010, *A&A*, 512, A15
- Rich, E. A., Wisniewski, J. P., Mayama, S., et al. 2015, *AJ*, 150, 86
- Rigliaco, E., Pascucci, I., Duchene, G., et al. 2015, *ApJ*, 801, 31
- Rodmann, J., Henning, T., Chandler, C. J., Mundy, L. G., & Wilner, D. J. 2006, *A&A*, 446, 211
- Rojas, G., Gregorio-Hetem, J., & Hetem, A. 2008, *MNRAS*, 387, 1335
- Romero, G. A., Schreiber, M. R., Cieza, L. A., et al. 2012, *ApJ*, 749, 79
- Rumble, D., Hatchell, J., Gutermuth, R. A., et al. 2015, *MNRAS*, 448, 1551
- Sallum, S., Follette, K. B., Eisner, J. A., et al. 2015, *Nature*, 527, 342
- Schneider, G., Wood, K., Silverstone, M. D., et al. 2003, *AJ*, 125, 1467
- Seifahrt, A., Neuhäuser, R., & Hauschildt, P. H. 2007, *A&A*, 463, 309
- Sestito, P., Palla, F., & Randich, S. 2008, *A&A*, 487, 965
- Siess, L., Dufour, E., & Forestini, M. 2000, *A&A*, 358, 593
- Silverstone, M. D., Meyer, M. R., Mamajek, E. E., et al. 2006, *ApJ*, 639, 1138
- Skrutskie, M. F., Cutri, R. M., Stiening, R., et al. 2006, *AJ*, 131, 1163
- Strom, K. M., Strom, S. E., Edwards, S., Cabrit, S., & Skrutskie, M. F. 1989, *AJ*, 97, 1451
- Suzuki, R., Kudo, T., Hashimoto, J., et al. 2010, in *Proc. SPIE*, Vol. 7735, 30
- Takagi, Y., Itoh, Y., & Oasa, Y. 2014, *PASJ*, 66, 88
- Tamura, M. 2009, 1158, 11
- Tamura, M., Suto, H., Itoh, Y., et al. 2000, in Society of Photo-Optical Instrumentation Engineers (SPIE) Conference Series, Vol. 4008, Optical and IR Telescope Instrumentation and Detectors, ed. M. Iye & A. F. Moorwood, 1153–1161
- Tanii, R., Itoh, Y., Kudo, T., et al. 2012, *PASJ*, 64, arXiv:1206.1215
- Testi, L., Skemer, A., Henning, T., et al. 2015, *ApJL*, 812, L38

- Thalmann, C., Grady, C. A., Goto, M., et al. 2010, *ApJL*, 718, L87
- Thalmann, C., Janson, M., Buenzli, E., et al. 2011, *ApJL*, 743, L6
- Thalmann, C., Mulders, G. D., Hodapp, K., et al. 2014, *A&A*, 566, A51
- Thalmann, C., Mulders, G. D., Janson, M., et al. 2015, *ApJL*, 808, L41
- Thomas, S. J., van der Blik, N. S., Rodgers, B., Doppmann, G., & Bouvier, J. 2007, in *IAU Symposium*, Vol. 240, IAU Symposium, ed. W. I. Hartkopf, P. Harmanec, & E. F. Guinan, 250–253
- Torres, C. A. O., Quast, G. R., Melo, C. H. F., & Sterzik, M. F. 2008, *Young Nearby Loose Associations*, ed. B. Reipurth, 757
- Torres, R. M., Loinard, L., Mioduszewski, A. J., et al. 2012, *ApJ*, 747, 18
- Torres, R. M., Loinard, L., Mioduszewski, A. J., & Rodríguez, L. F. 2007, *ApJ*, 671, 1813
- , 2009, *ApJ*, 698, 242
- Trotta, F., Testi, L., Natta, A., Isella, A., & Ricci, L. 2013, *A&A*, 558, A64
- Tsukagoshi, T., Saito, M., Kitamura, Y., et al. 2011, *ApJ*, 726, 45
- Tsukagoshi, T., Momose, M., Hashimoto, J., et al. 2014, *ApJ*, 783, 90
- Valenti, J. A., Basri, G., & Johns, C. M. 1993, *AJ*, 106, 2024
- van Boekel, R., Min, M., Waters, L. B. F. M., et al. 2005, *A&A*, 437, 189
- van der Marel, N., van Dishoeck, E. F., Bruderer, S., et al. 2016, *A&A*, 585, A58
- van der Marel, N., van Dishoeck, E. F., Bruderer, S., & van Kempen, T. A. 2014, *A&A*, 563, A113
- van der Marel, N., van Dishoeck, E. F., Bruderer, S., et al. 2013, *Science*, 340, 1199
- van der Plas, G., van den Ancker, M. E., Fedele, D., et al. 2008, *A&A*, 485, 487
- van Leeuwen, F. 2007, *A&A*, 474, 653
- Verhoeff, A. P., Min, M., Pantin, E., et al. 2011, *A&A*, 528, A91
- Vieira, S. L. A., Corradi, W. J. B., Alencar, S. H. P., et al. 2003, *AJ*, 126, 2971
- Wahhaj, Z., Cieza, L., Koerner, D. W., et al. 2010, *ApJ*, 724, 835
- Walker, G. A., Walker, A. R., Racine, R., Fletcher, M. J., & McClure, R. D. 1994, *PASP*, 106, 356
- Walter, F. M., Vrba, F. J., Mathieu, R. D., Brown, A., & Myers, P. C. 1994, *AJ*, 107, 692
- Webb, R. A., Zuckerman, B., Platais, I., et al. 1999, *ApJL*, 512, L63
- Weinberger, A. J., Becklin, E. E., Schneider, G., et al. 2002, *ApJ*, 566, 409
- White, R. J., & Basri, G. 2003, *ApJ*, 582, 1109
- White, R. J., & Ghez, A. M. 2001a, *ApJ*, 556, 265
- , 2001b, *ApJ*, 556, 265
- White, R. J., Ghez, A. M., Reid, I. N., & Schultz, G. 1999, *ApJ*, 520, 811
- White, R. J., & Hillenbrand, L. A. 2004, *ApJ*, 616, 998
- Wichmann, R., Bastian, U., Krautter, J., Jankovics, I., & Rucinski, S. M. 1998, *MNRAS*, 301, 39L
- Wichmann, R., Covino, E., Alcalá, J. M., et al. 1999, *MNRAS*, 307, 909
- Wichmann, R., Krautter, J., Schmitt, J. H. M. M., et al. 1996, *A&A*, 312, 439
- Wichmann, R., Torres, G., Melo, C. H. F., et al. 2000, *A&A*, 359, 181
- Wilking, B. A., Greene, T. P., Lada, C. J., Meyer, M. R., & Young, E. T. 1992, *ApJ*, 397, 520
- Wilking, B. A., McCaughrean, M. J., Burton, M. G., et al. 1997, *AJ*, 114, 2029
- Wilking, B. A., Meyer, M. R., Robinson, J. G., & Greene, T. P. 2005, *AJ*, 130, 1733
- Williams, J. P., & Cieza, L. A. 2011, *Annual Review of A&A*, 49, 67
- Yamamoto, K., Matsuo, T., Shibai, H., et al. 2013, *PASJ*, 65, arXiv:1306.3100
- Yang, Y., Hashimoto, J., Hayashi, S. S., et al. 2016, *ArXiv e-prints*, arXiv:1610.09134
- Yudin, R. V., Clarke, D., & Smith, R. A. 1999, *A&A*, 345, 547
- Zacharias, N., Finch, C. T., Girard, T. M., et al. 2012, *VizieR Online Data Catalog*, 1322
- Zacharias, N., Monet, D. G., Levine, S. E., et al. 2005, *VizieR Online Data Catalog*, 1297
- Zacharias, N., Urban, S. E., Zacharias, M. I., et al. 2003, *VizieR Online Data Catalog*, 1289
- Zuckerman, B., Webb, R. A., Schwartz, M., & Becklin, E. E. 2001, *ApJL*, 549, L233